SUPPORTING INFORMATION

Mono- and Dinuclear Coinage Metal Complexes Supported by an Imino-Pyridine NHC Ligand: Structural and Photophysical Studies

Thomas Simler,*[,†] Karen Möbius,[†] Kerstin Müller,[†] Thomas J. Feuerstein,[†] Michael T. Gamer,[†] Sergei Lebedkin,[‡] Manfred M. Kappes[‡,§] and Peter W. Roesky*[,†]

[†] *Institute of Inorganic Chemistry, Karlsruhe Institute of Technology (KIT), Engesserstr. 15, 76131 Karlsruhe, Germany E-mail: thomas.simler@kit.edu, roesky@kit.edu*

[‡] *Institute of Nanotechnology, Karlsruhe Institute of Technology (KIT), Hermann-von-Helmholtz-Platz 1, 76344 Eggenstein-Leopoldshafen, Germany*

[§] *Institute of Physical Chemistry, Karlsruhe Institute of Technology (KIT), Fritz-Haber Weg 2, 76131 Karlsruhe, Germany*

Content

I. SYNTHESIS AND CHARACTERIZATION

I.1. Synthesis of 2-acetyl-6-bromopyridine (1)

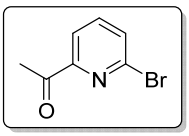

This compound was synthesized according to the literature procedure.[1]

To a solution of 2,6-dibromopyridine (23.7 g, 100 mmol) in Et_2O (300 mL), cooled at -78 °C, was added dropwise a solution of *n*BuLi in hexane (42 mL of a 2.5 M hexane solution, 105 mmol) over 15 min. After stirring at -78 °C for 30 min, a solution of DMA (10.2 mL, 9.58 g, 110 mmol) in Et_2O (50 mL) was slowly added. The resulting mixture was stirred at -78 °C for 20 min, let warm up to r.t., further stirred for 2 h and quenched by addition of 10% aqueous HCl until acidic. The resulting solution was made alkaline by addition of 10% aqueous K_2CO_3 solution. The aqueous layer was separated and extracted with diethyl ether (3 x 50 mL). The combined organic extracts were washed with brine and dried over $MgSO_4$. Evaporation of the volatiles under reduced pressure gave the crude product as a yellow oil slowly crystallizing under vacuum. Recrystallization from Et_2O/hexane afforded the title compound as colorless crystals. Yield: 15.9 g (79.5 mmol), 80%.

^{1}H NMR (400.30 MHz, $CDCl_3$): δ [ppm]: 7.98 (dd, $^3J_{HH}$ = 7.1 Hz, $^4J_{HH}$ = 1.0 Hz, 1H, C$H_{pyr.}$), 7.72-7.63 (m, 2H, C$H_{pyr.}$), 2.70 (s, 3H, CH_3). These data are consistent with those described in the literature.[1b]

I.2. Synthesis of 2-bromo-6-(2-methyl-1,3-dioxolan-2-yl)pyridine (2)

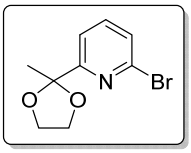

This compound was synthesized using a slightly modified literature procedure.[1a,2]

A mixture of **1** (21.0 g, 105 mmol), ethylene glycol (6.5 mL, 7.20 g, 116 mmol), *p*-toluenesulfonic acid monohydrate (1.00 g, 5.25 mmol, 5 mol%) in cyclohexane was heated to reflux under Dean-Stark conditions for 5 h. To the resulting solution, cooled to room temperature, was added aqueous K_2CO_3 solution. The aqueous layer was separated and extracted with diethyl ether (3 x 100 mL). The combined organic extracts were washed with brine and dried over $MgSO_4$. Evaporation of the solvent under reduced pressure gave the crude product as a light brown oil (crude yield: 24.6 g (101 mmol), 96%). A microcrystalline white product could be obtained by keeping a concentrated Et_2O/pentane solution of the product at -40 °C for several days. Yield of the crystals: 15.9 g (65.1 mmol), 62%. **^{1}H NMR** (400.30 MHz, $CDCl_3$): δ [ppm]: 7.54-7.43 (m, 2H, C$H_{pyr.}$), 7.40 (dd, $^3J_{HH}$ = 7.3 Hz, $^4J_{HH}$ = 1.5 Hz, 1H, C$H_{pyr.}$), 4.13-3.83 (m, 4H, OCH_2), 1.71 (s, 3H, CH_3). These data are consistent with those described in the literature.[2]

I.3. Synthesis of (6-(2-methyl-1,3-dioxolan-2-yl)pyridin-2-yl)methanol (3)

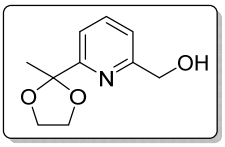

The synthesis of **3** has already been reported in a WO Patent but no NMR characterization has been provided.[3]

To a solution of **2** (8.00 g, 32.8 mmol) in Et_2O (100 mL), cooled at -78 °C, was added dropwise a solution of *n*BuLi in hexane (13.8 mL of a 2.5 M hexane solution, 34.5 mmol). After stirring at -78 °C for 30 min, a solution of DMF (2.8 mL, 2.65 g, 36.2 mmol) in Et_2O (20 mL) was slowly added. The resulting mixture was allowed to warm up to 0 °C, stirred for 1.5 h and quenched by addition of methanol (10 mL). $NaBH_4$ (1.86 g, 49.2 mmol) was added and the reaction mixture was allowed to reach r.t. and further stirred for 1 h. The excess $NaBH_4$ was quenched by addition of 10% aqueous HCl until acidic and the resulting solution was made alkaline by addition of K_2CO_3. The reaction mixture was concentrated under reduced pressure and extracted with CH_2Cl_2 (3 x 50 mL). The combined organic extracts were washed with brine and dried over $MgSO_4$. Evaporation of the volatiles under reduced pressure gave the crude product as a yellow oil slowly crystallizing under vacuum. Recrystallization from CH_2Cl_2/Et_2O at -40 °C afforded the title compound as a pale yellow solid. Yield: 5.37 g (27.5 mmol), 84%.

^{1}H NMR (300.13 MHz, $CDCl_3$): δ [ppm]: 7.70 (t, $^3J_{HH}$ = 7.7 Hz, 1H, *p*-C*H*$_{pyr.}$), 7.47 (dm, $^3J_{HH}$ = 7.7 Hz, 1H, *m*-C*H*$_{pyr.}$), 7.20 (dm, $^3J_{HH}$ = 7.8 Hz, 1H, *m*-C*H*$_{pyr.}$), 4.78 (s, 2H, C*H*$_2$OH), 4.16-3.83 (m, 4H, OC*H*$_2$), 3.51 (br s, 1H, O*H*), 1.74 (s, 3H, C*H*$_3$).

^{13}C{^{1}H} NMR (75.47 MHz, $CDCl_3$): δ [ppm]: 159.8 (*C*$_{pyr}$), 159.0 (*C*$_{pyr.}$), 137.6 (*C*H$_{pyr.}$), 120.0 (*C*H$_{pyr.}$), 118.2 (*C*H$_{pyr.}$), 108.6 (*C*CH$_3$), 65.2 (O*C*H$_2$), 64.2 (*C*H$_2$OH), 25.3 (*C*H$_3$).

II. X-RAY CRYSTALLOGRAPHY

II.1. Special comments

The following special comments apply to the models of the structures:

- The asymmetric unit of **8**·CH_2Cl_2 contains one molecule of CH_2Cl_2 disordered over two positions with an occupancy ratio of 0.6667/0.3333.
- For **11**, the C_6F_5 moiety is disordered over two positions with an occupancy ratio of 0.5/0.5.
- The asymmetric unit of **12**·0.25(CH_2Cl_2) contains one half molecule of the complex and 0.125 molecule of CH_2Cl_2. The two *i*Pr groups (C27-C29, C30-C32) and the mesityl group (N4, C12-C20) are disordered over two positions with an occupancy ratio of 0.5/0.5. The half BF_4 anion is disordered over two positions with an occupancy ratio of 0.25/0.25.
- The asymmetric unit of **13**·0.5(CH_2Cl_2) contains one half molecule of the complex and 0.25 molecule of CH_2Cl_2. The mesityl group (N4, C12-C20) is disordered over two positions with an occupancy ratio of 0.5/0.5. The half BF_4 anion is disordered over two positions with an occupancy ratio of 0.25/0.25
- In the structure of **14**, one BF_4 anion is disordered over two positions with an occupancy ratio of 0.75/0.25. One *i*Pr group (C27-C29) and one DiPP group (C53-C64) are disordered over two positions with an occupancy ratio of 0.5/0.5. An alert A (VERY LARGE Solvent Accessible VOID(S) in Structure) arises in the Checkcif but the voids look like flat, twisted tunnels through the unit cell and no electron density can be observed within. It seems that without a change of the molecule packing, none of the available solvent molecules (or BF_4^-) will fit inside.
- The asymmetric unit of **15**·MeCN contains two molecules of the complex and two molecules of MeCN. The crystals were twinned and an hklf5 was generated via STOE twin integration (BASF 0.345).
- The asymmetric unit of **17**·3(MeCN) contains half a molecule of the complex and 1.5 molecules of MeCN; the BF_4 anion is disordered over two positions with an occupancy ratio of 0.5/0.5.
- The asymmetric unit of **18**·0.5(CH_2Cl_2) contains half a molecule of the complex and 0.25 disordered molecule of CH_2Cl_2. The BF_4 anion is disordered over two positions with an occupancy ratio of 0.75/0.25.

II.2. Summary of crystal data

Table S1. Crystal data, data collection and refinement for compounds **8**-**12**.

Compounds	**8**·CH_2Cl_2	**9**	**10**	**11**	**12**·0.25 (CH_2Cl_2)
Chemical formula	$C_{32}H_{39}BrN_4$·CH_2Cl_2	$C_{32}H_{38}AgBrN_4$	$C_{32}H_{38}AuIN_4$	$C_{38}H_{38}AuF_5N_4$	$C_{64}H_{76}AgBF_4N_8$·0.25(CH_2Cl_2)
CCDC Number	1935666	1935667	1935668	1935670	1935669
Formula Mass	644.51	666.44	802.53	842.69	1173.23
Crystal system	Monoclinic	Monoclinic	Triclinic	Orthorhombic	Tetragonal
a/Å	8.8560(4)	22.9267(10)	8.5375(3)	15.8416(5)	15.8586(8)
b/Å	30.4059(10)	8.9889(3)	9.2775(3)	25.5241(8)	15.8586(8)
c/Å	12.8631(6)	14.7832(6)	23.0315(12)	17.8219(8)	24.954(2)
α/°			98.830(4)		
β/°	97.550(3)	95.304(3)	93.693(4)		
γ/°			110.788(3)		
Unit cell volume/Å^3	3433.7(3)	3033.6(2)	1671.26(12)	7206.2(5)	6275.8(8)
Radiation type	MoKα	MoKα	MoKα	MoKα	MoKα
Wavelength/Å	0.71073	0.71073	0.71073	0.71073	0.71073
Temperature/K	200	100	210	150	100
Space group	$P2_1/n$	$P2_1/c$	$P\bar{1}$	$Pbca$	$P4/n$
Z	4	4	2	8	4
Absorption coefficient, μ/mm	1.379	2.008	5.349	4.141	0.399
No. of reflections measured	21976	16460	18062	72523	16632
No. of independent reflections	6414	7496	9266	10053	7896
R_{int}	0.0267	0.0410	0.0611	0.0705	0.0236
Final R_1 values ($I > 2\,\sigma(I)$)	0.0458	0.0396	0.0588	0.0246	0.0409
Final $wR(F^2)$ values ($I > 2\,\sigma(I)$)	0.1056	0.0937	0.1376	0.0454	0.1085
Final R_1 values (all data)	0.0733	0.0644	0.1151	0.0801	0.0751
Final $wR(F^2)$ values (all data)	0.1224	0.1026	0.1642	0.0534	0.1230
Goodness of fit on F^2	1.055	0.956	0.983	0.859	1.037

Table S2. Crystal data, data collection and refinement for compounds **13**-**15, 17** and **18**.

Compounds	**13**·0.5(CH_2Cl_2)	**14**	**15**·MeCN	**17**·3(MeCN)	**18**·0.5(CH_2Cl_2)
Chemical formula	$C_{64}H_{76}AuBF_4N_8$·0.5(CH_2Cl_2)	$C_{64}H_{78}B_3CuF_{12}N_8$	$C_{64}H_{76}Ag_2B_2F_8N_8$·$C_2H_3N$	$C_{64}H_{76}AgAuB_2F_8N_8$·3($C_2H_3N$)	$C_{64}H_{76}AuB_2CuF_8N_8$·0.5($CH_2Cl_2$)
CCDC Number	1935671	1935672	1935673	1935674	1935675
Formula Mass	1283.56	1283.31	1387.74	1558.94	1433.91
Crystal system	Tetragonal	Monoclinic	Monoclinic	Monoclinic	Monoclinic
a/Å	15.8559(5)	14.2894(6)	28.7223(7)	16.8577(5)	11.2005(5)
b/Å	15.8559(5)	29.2539(10)	14.6522(4)	26.5165(7)	32.4978(10)
c/Å	24.8751(9)	18.1940(6)	34.0236(7)	15.9894(3)	19.2893(7)
α/°					
β/°		111.649(3)	112.457(2)	98.631(2)	98.819(3)
γ/°					
Unit cell volume/Å^3	6253.8(5)	7069.0(5)	13232.8(6)	7066.4(3)	6938.1(5)
Radiation type	MoKα	GaKα	MoKα	MoKα	MoKα
Wavelength/Å	0.71073	1.34143	0.71073	0.71073	0.71073
Temperature/K	100	150	150	150	150
Space group	$P4/n$	$P2_1/n$	$P2_1/n$	$C2/c$	$C2/c$
Z	4	4	8	4	4
Absorption coefficient, μ/mm	2.452	2.067	0.661	2.420	2.521
No. of reflections measured	16277	37374	138299	18696	19360
No. of independent reflections	7818	13156	138299	9722	9623
R_{int}	0.0356	0.0917	Refined as a 2-component twin	0.0283	0.0581
Final R_1 values ($I > 2\sigma(I)$)	0.0373	0.1123	0.0415	0.0402	0.0575
Final $wR(F^2)$ values ($I > 2\sigma(I)$)	0.0946	0.2855	0.1030	0.1025	0.1408
Final R_1 values (all data)	0.0610	0.1980	0.0710	0.0514	0.0834
Final $wR(F^2)$ values (all data)	0.1091	0.3284	0.1176	0.1091	0.1408
Goodness of fit on F^2	1.025	1.001	0.995	1.104	0.996

II.3. Crystal structures

II.3.1. The molecular structure of 8 in the solid state

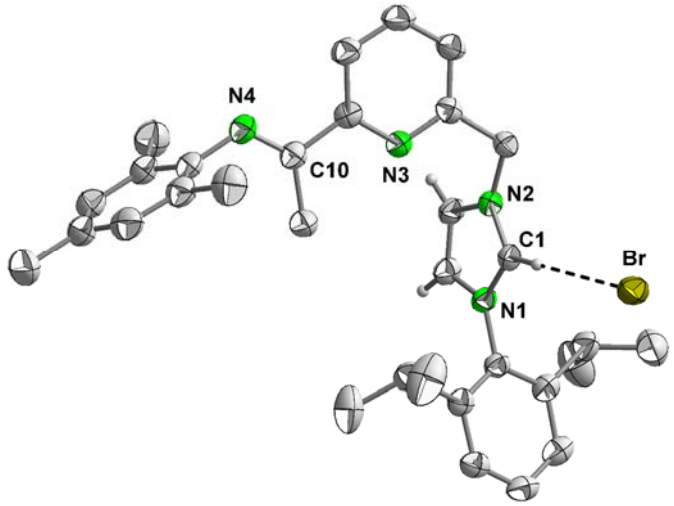

Figure S1. Molecular structure of **8** in the solid state with thermal ellipsoids at the 40% probability level. H atoms, except for the imidazolium moiety, and non-coordinating solvent molecules are omitted for clarity. Selected bond distances (Å) and angles [°]: N1-C1 1.334(4), N2-C1 1.326(4), N4-C10 1.266(4); N2-C1-N1 108.4(2).

II.3.2. The molecular structure of 9 in the solid state

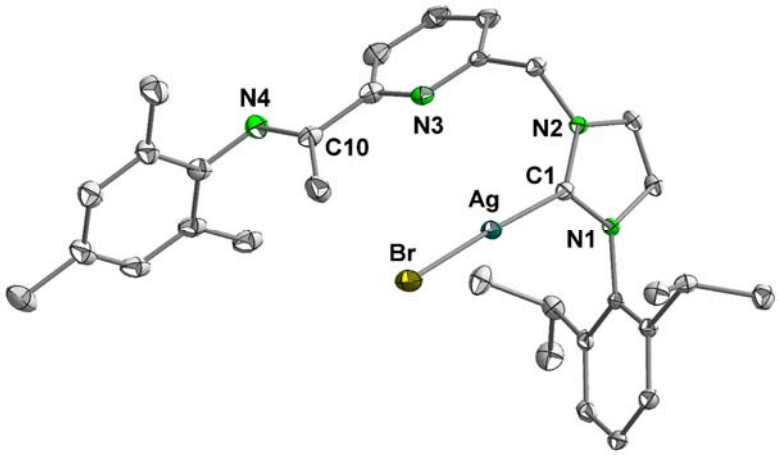

Figure S2. Molecular structure of **9** in the solid state with thermal ellipsoids at the 50% probability level. H atoms are omitted for clarity. Selected bond distances (Å) and angles [°]: Ag-Br 2.4332(4), Ag-C1 2.078(3), N1-C1 1.350(4), N2-C1 1.351(4), N4-C10 1.277(5); C1-Ag-Br 177.24(9), N1-C1-N2 104.4(3).

II.3.3. The molecular structure of 10 in the solid state

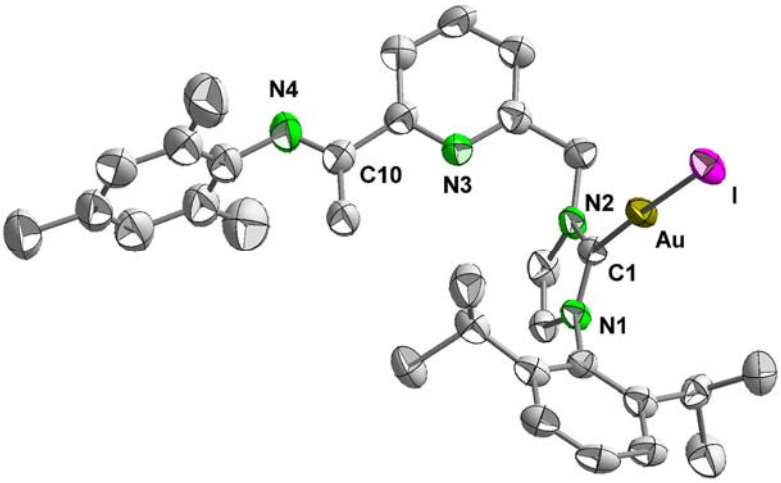

Figure S3. Molecular structure of **10** in the solid state with thermal ellipsoids at the 40% probability level. H atoms are omitted for clarity. Selected bond distances (Å) and angles [°]: Au-I 2.5437(7), Au-C1 1.999(9), N1-C1 1.349(10), N2-C1 1.333(10), C10-N4 1.295(14); C1-Au-I 177.7(2), N2-C1-N1 105.3(7).

II.3.4. The molecular structure of 11 in the solid state

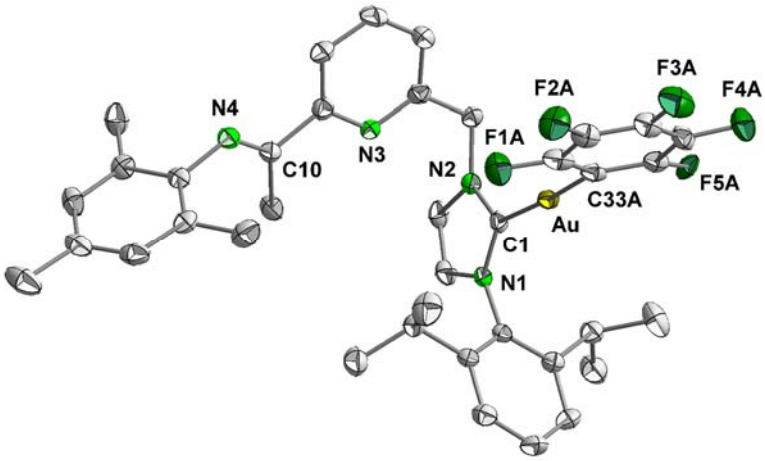

Figure S4. Molecular structure of **11** in the solid state with thermal ellipsoids at the 50% probability level. H atoms are omitted for clarity. Only one disordered position of the C_6F_5 group is depicted for clarity. Selected bond distances (Å) and angles [°]: Au-C1 2.011(3), Au-C33A 2.054(7), N1-C1 1.357(4), N2-C1 1.344(3), N4-C10 1.266(4); C1-Au-C33A 175.8(4), N2-C1-N1 104.3(2).

II.3.5. The molecular structure of 12 in the solid state

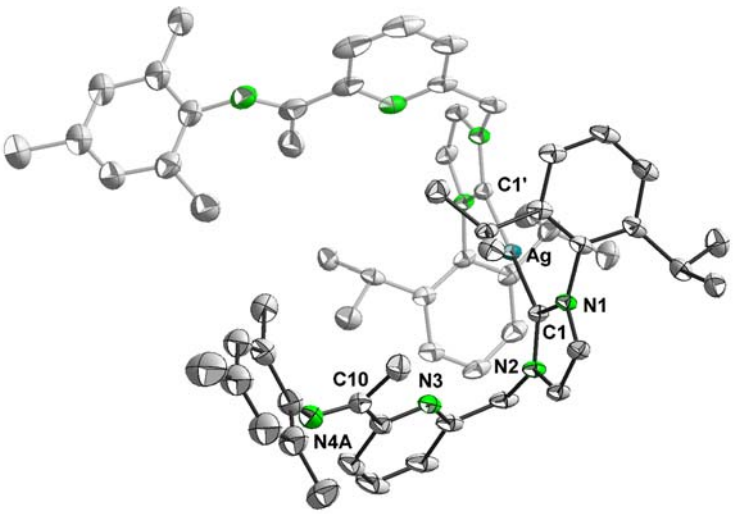

Figure S5. Molecular structure of the cation of **12** in the solid state with thermal ellipsoids at the 40% probability level. H atoms and non-coordinating solvent molecules are omitted and only one disordered position of the mesityl and *i*Pr groups is depicted for clarity. Selected bond distances (Å) and angles [°]: Ag-C1 2.066(2), N1-C1 1.357(3), N2-C1 1.344(3), N4A-C10 1.36(2); C1-Ag-C1' 179.38(12), N2-C1-N1 104.0(2). Atoms with the prime character in the atom labels (') are at equivalent positions (1/2-x, 3/2-y, z).

II.3.6. The molecular structure of 13 in the solid state

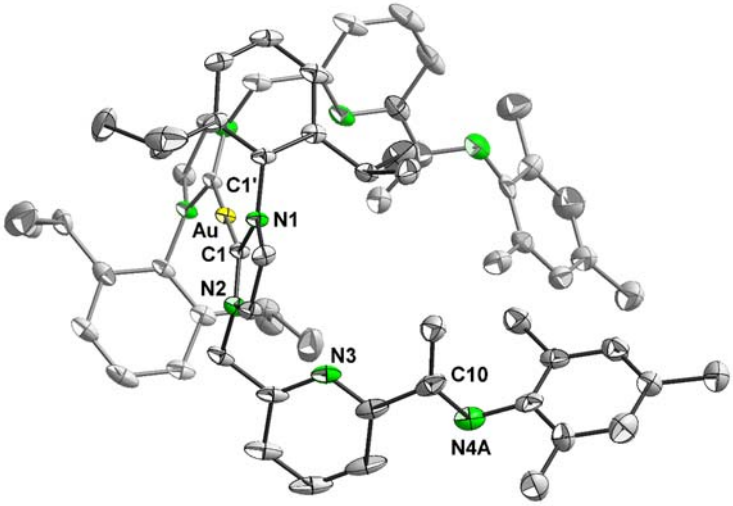

Figure S6. Molecular structure of the cation of **13** in the solid state with thermal ellipsoids at the 40% probability level. H atoms and non-coordinating solvent molecules are omitted and only one disordered position of the mesityl group is depicted for clarity. Selected bond distances (Å) and angles [°]: Au-C1 2.020(3), N1-C1 1.358(4), N2-C1 1.337(5), N4A-C10 1.297(11); C1-Au-C1' 179.4(2), N2-C1-N1 105.0(3). Atoms with the prime character in the atom labels (') are at equivalent positions (1/2-x, 3/2-y, z).

II.3.7. The molecular structure of 14 in the solid state

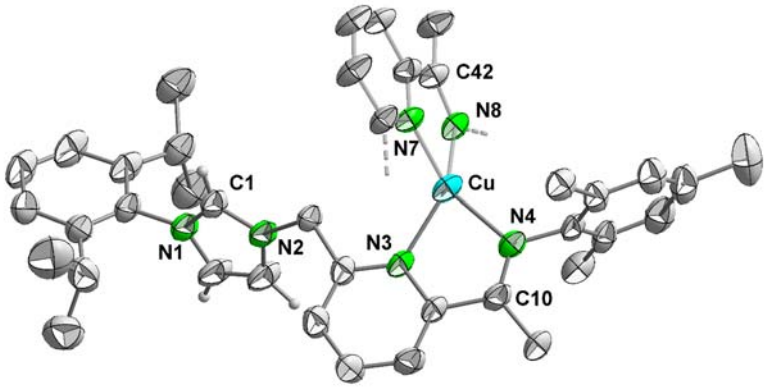

Figure S7. Molecular structure of the cation of **14** in the solid state with thermal ellipsoids at the 40% probability level. H atoms, except for the imidazolium moiety, are omitted for clarity. Only the imino-pyridine moiety of the upper ligand and one disordered position of the *i*Pr groups are depicted for clarity. Selected bond distances (Å) and angles [°]: Cu-N3 2.045(5), Cu-N4 2.012(5), Cu-N7 2.068(5), Cu-N8 2.010(5), N1-C1 1.320(8), N2-C1 1.327(7), N4-C10 1.278(8), N8-C42 1.309(7); N4-Cu-N3 80.5(2), N8-Cu-N7 81.1(2), N3-Cu-N7 112.9(2), N4-Cu-N7 133.5(2), N8-Cu-N3 134.5(2), N8-Cu-N4 122.2(2), N1-C1-N2 108.0(5).

II.3.8. The molecular structure of 15 in the solid state

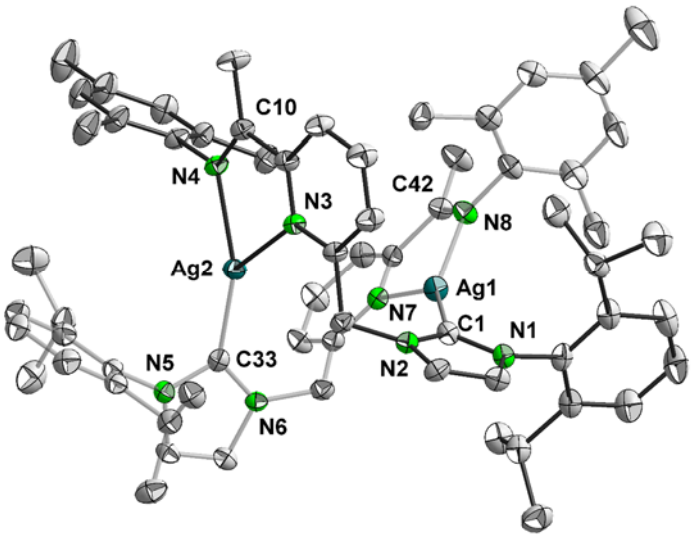

Figure S8. Molecular structure of the cation of **15** in the solid state with thermal ellipsoids at the 40% probability level. H atoms and non-coordinating solvent molecules are omitted for clarity. Selected bond distances (Å) and angles [°]: Ag1-N7 2.385(4), Ag1-N8 2.260(4), Ag1-C1 2.090(5), Ag2-N3 2.383(4), Ag2-N4 2.251(4), Ag2-C33 2.083(5), N1-C1 1.356(6), N2-C1 1.360(6), N4-C10 1.288(6), N8-C42 1.284(6); N8-Ag1-N7 70.52(14), C1-Ag1-N7 141.2(2), C1-Ag1-N8 148.2(2), N4-Ag2-N3 71.53(14), C33-Ag2-N3 135.1(2), C33-Ag2-N4 153.1(2), N1-C1-N2 104.3(4), N6-C33-N5 104.5(4). The asymmetric unit of **15**·MeCN contains two molecules of **15** with very similar metrical data.

II.3.9. The molecular structure of 17 in the solid state

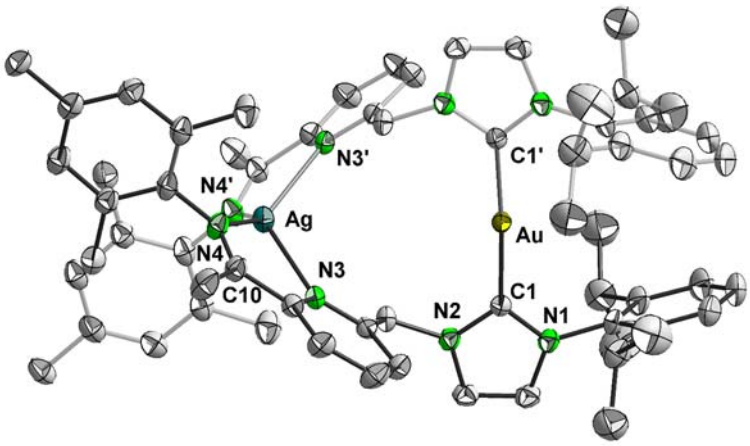

Figure S9. Molecular structure of the cation of **17** in the solid state with thermal ellipsoids at the 40% probability level. H atoms and non-coordinating solvent molecules are omitted for clarity. Selected bond distances (Å) and angles [°]: Au1-C1 2.014(3), Ag2-N3 2.360(3), Ag2-N4 2.278(3), N1-C1 1.343(5), N2-C1 1.352(5), N4-C10 1.287(5); C1-Au1-C1' 176.4(2), N3-Ag2-N3' 117.74(14), N4-Ag2-N3' 133.09(12), N4-Ag2-N3 71.96(11), N4-Ag2-N4' 137.7(2), N1-C1-N2 104.6(3). Atoms with the prime character in the atom labels (') are at equivalent positions (-x, y, 3/2-z).

II.3.10. The molecular structure of 18 in the solid state

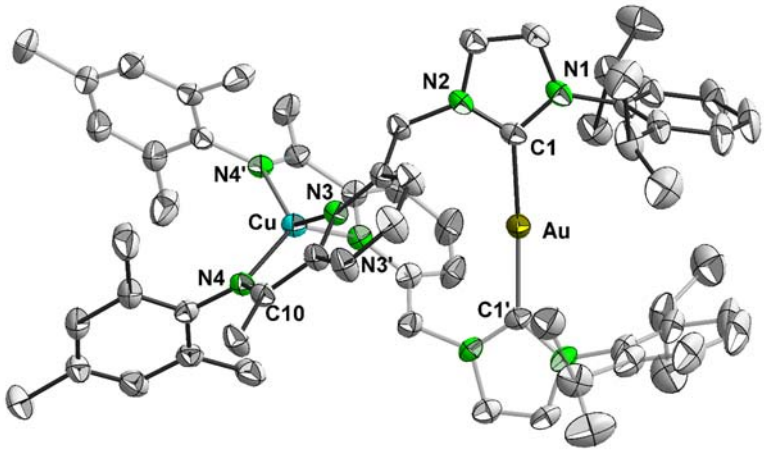

Figure S10. Molecular structure of the cation of **18** in the solid state with thermal ellipsoids at the 40% probability level. H atoms and non-coordinating solvent molecules are omitted for clarity. Selected bond distances (Å) and angles [°]: Au-C1 2.031(5), Cu-N3 2.053(4), Cu-N4 2.009(4), N1-C1 1.335(6), N2-C1 1.334(6), N4-C10 1.289(6); C1-Au-C1' 176.7(3), N3-Cu-N3' 110.0(2), N4-Cu-N3' 133.35(15), N4-Cu-N3 81.31(15), N4-Cu-N4' 124.4(2), N2-C1-N1 106.1(4). Atoms with the prime character in the atom labels (') are at equivalent positions (1-x, y, 1/2-z).

II.3.11. Preliminary molecular structure of 16 in the solid state

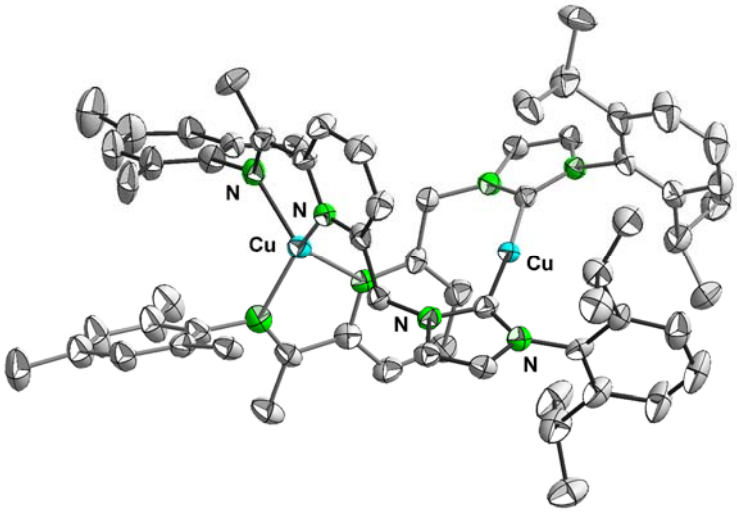

Figure S11. Preliminary molecular structure of the cation of **16** in the solid state with thermal ellipsoids at the 40% probability level. H atoms and non-coordinating solvent molecules are omitted for clarity. The data set acquired did not allow the refinement of the structural model under acceptable *R* values but confirmed the connectivity of the atoms.

Cell parameters: a = 12.029(1), b = 17.707(2), c = 18.021(2) Å; α = 88.327(6), β = 84.908(6), γ = 70.053(6)°; V = 3593.9(5) Å^3.

III. NMR SPECTRA

III.1. Compound 3

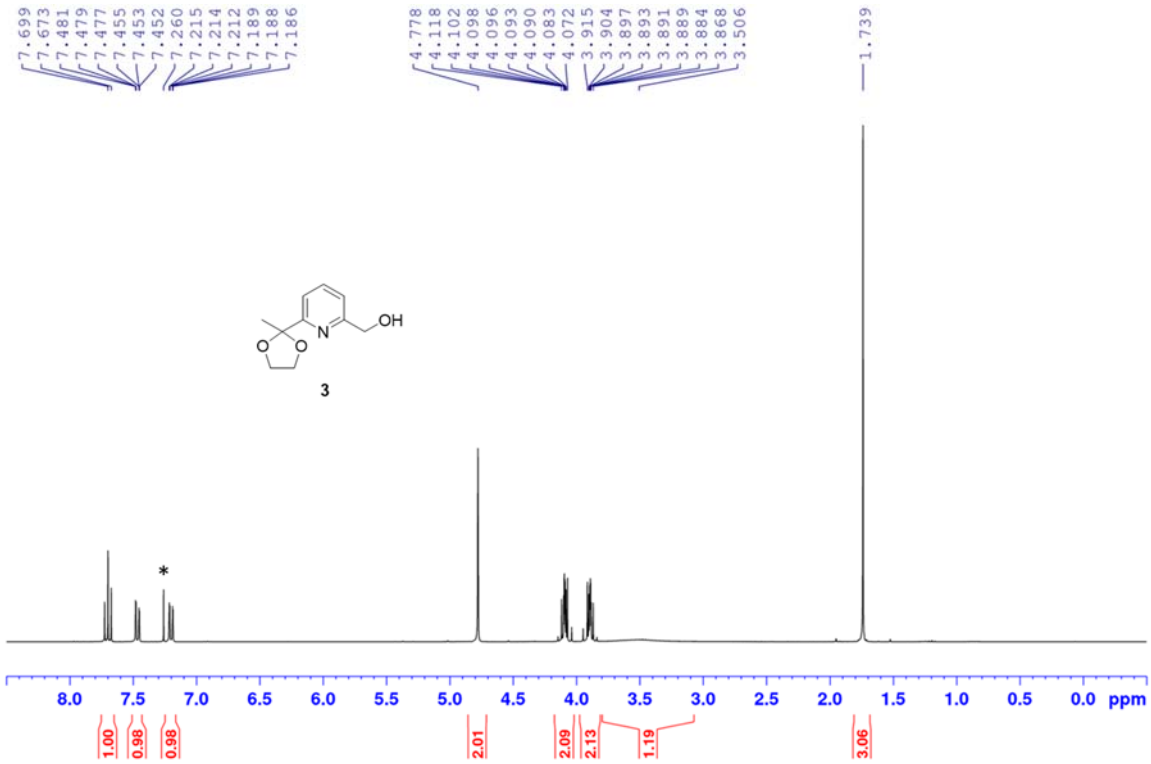

Figure S12. ^{1}H NMR spectrum of **3** in $CDCl_3$ (residual protio solvent from $CDCl_3$ at δ7.26 (*)).

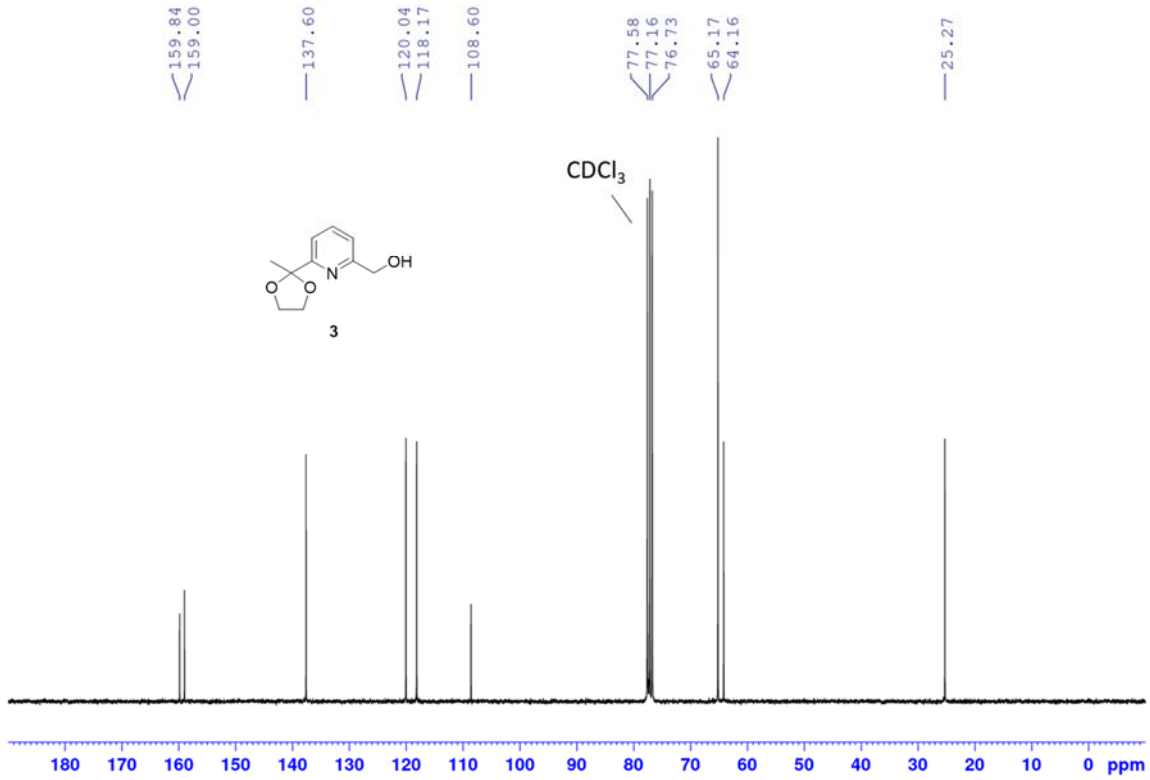

Figure S13. ^{13}C{^{1}H} NMR spectrum of **3** in $CDCl_3$ (solvent signal at δ77.16).

III.2. Compound 4

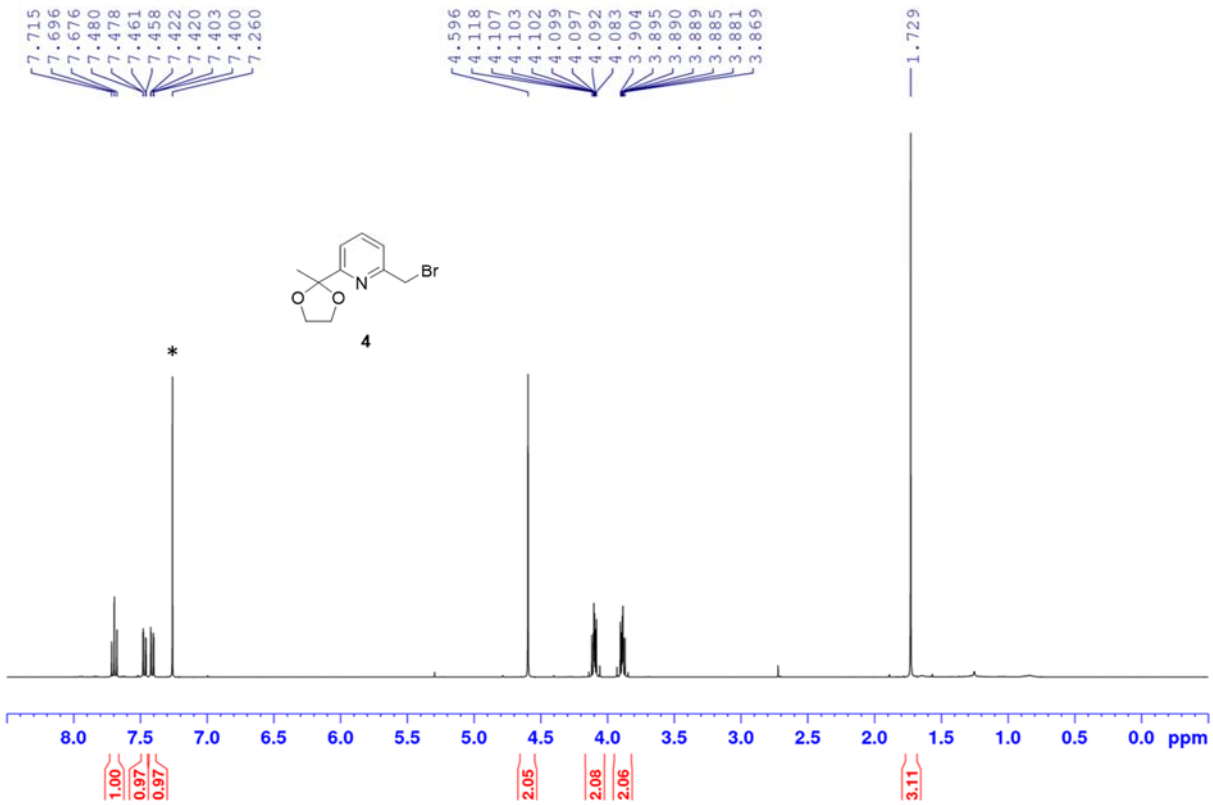

Figure S14. ^{1}H NMR spectrum of **4** in $CDCl_3$ (residual protio solvent from $CDCl_3$ at δ7.26 (*)).

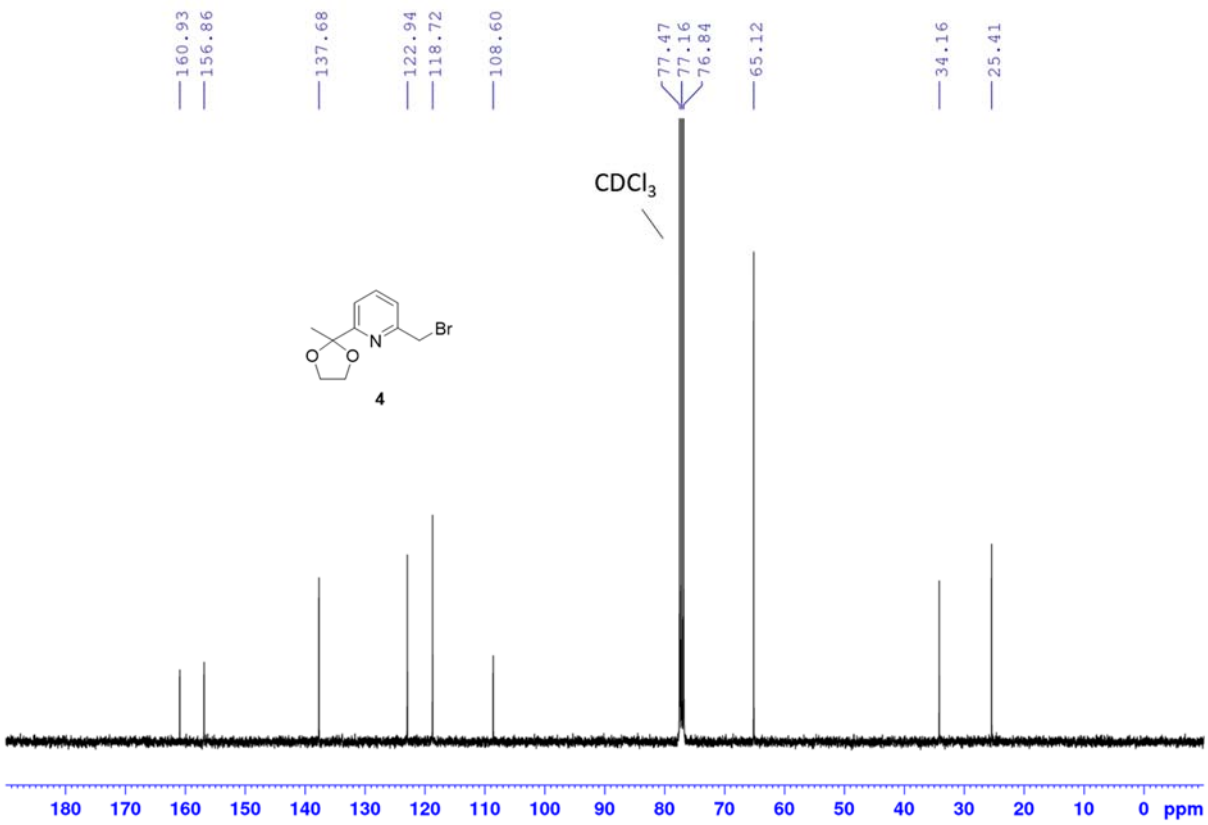

Figure S15. ^{13}C{^{1}H} NMR spectrum of **4** in $CDCl_3$ (solvent signal at δ77.16).

III.3. Compound 6

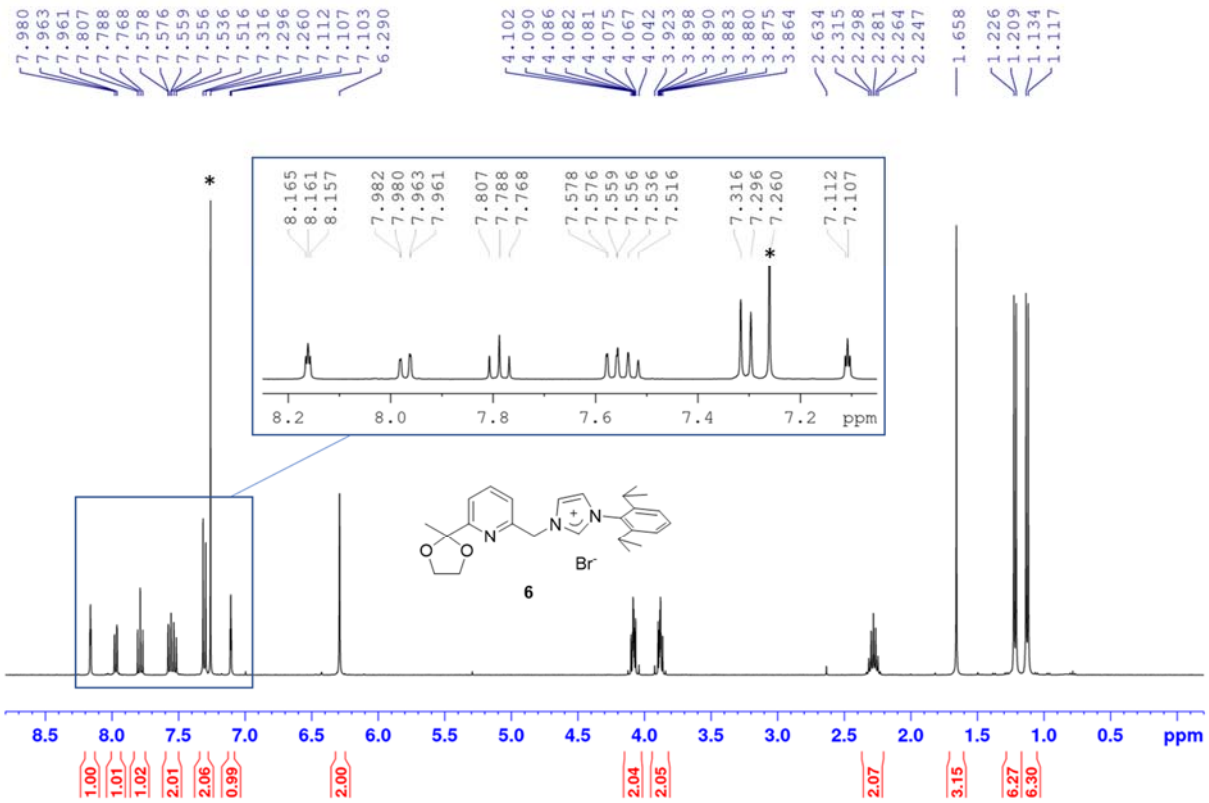

Figure S16. ^{1}H NMR spectrum of **6** in $CDCl_3$ (residual protio solvent from $CDCl_3$ at δ7.26 (*)).

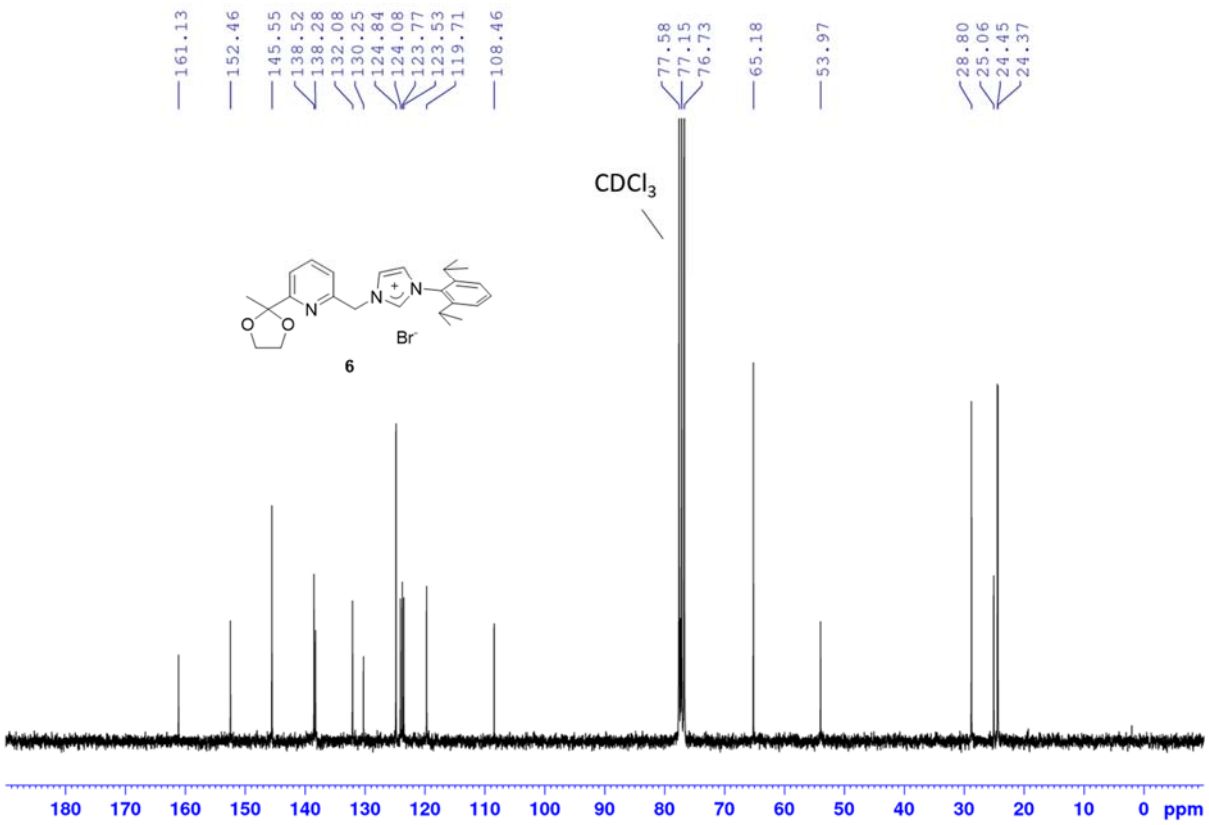

Figure S17. ^{13}C{^{1}H} NMR spectrum of **6** in $CDCl_3$ (solvent signal at δ77.15).

III.4. Compound 7

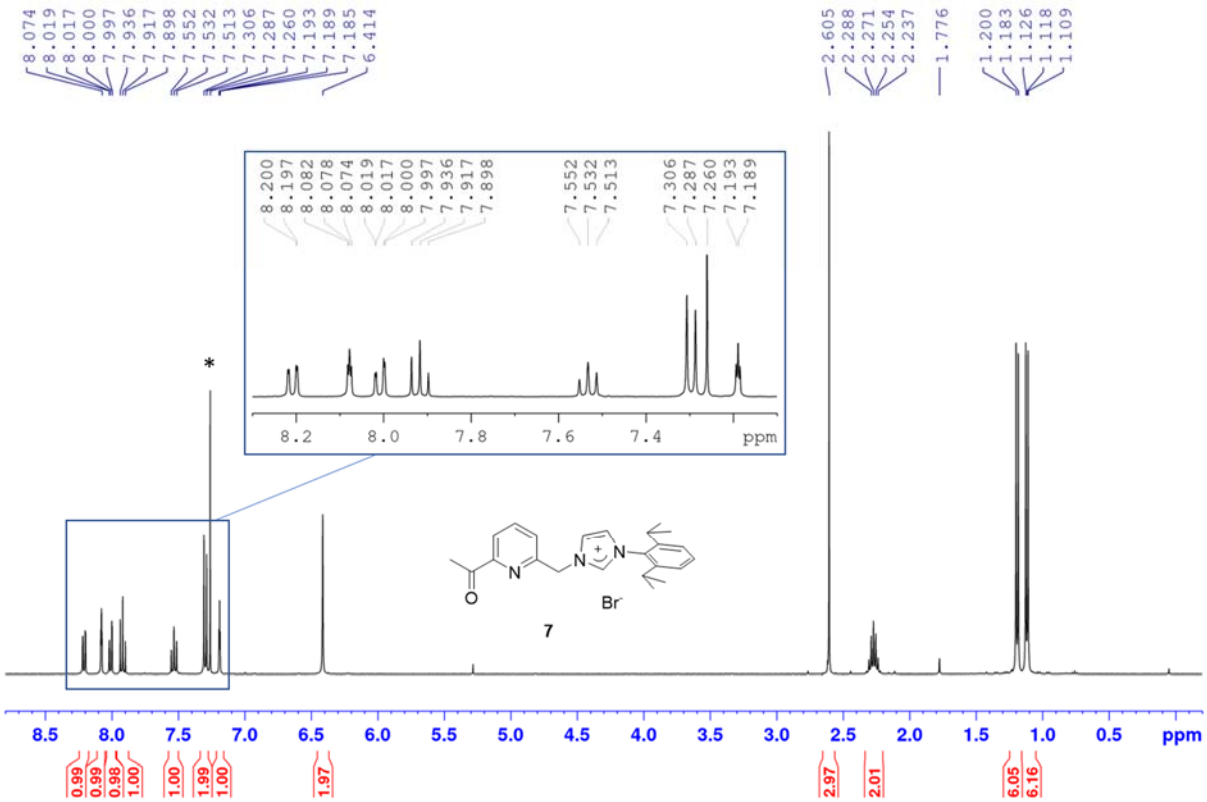

Figure S18. ^{1}H NMR spectrum of **7** in $CDCl_3$ (residual protio solvent from $CDCl_3$ at δ7.26 (*)).

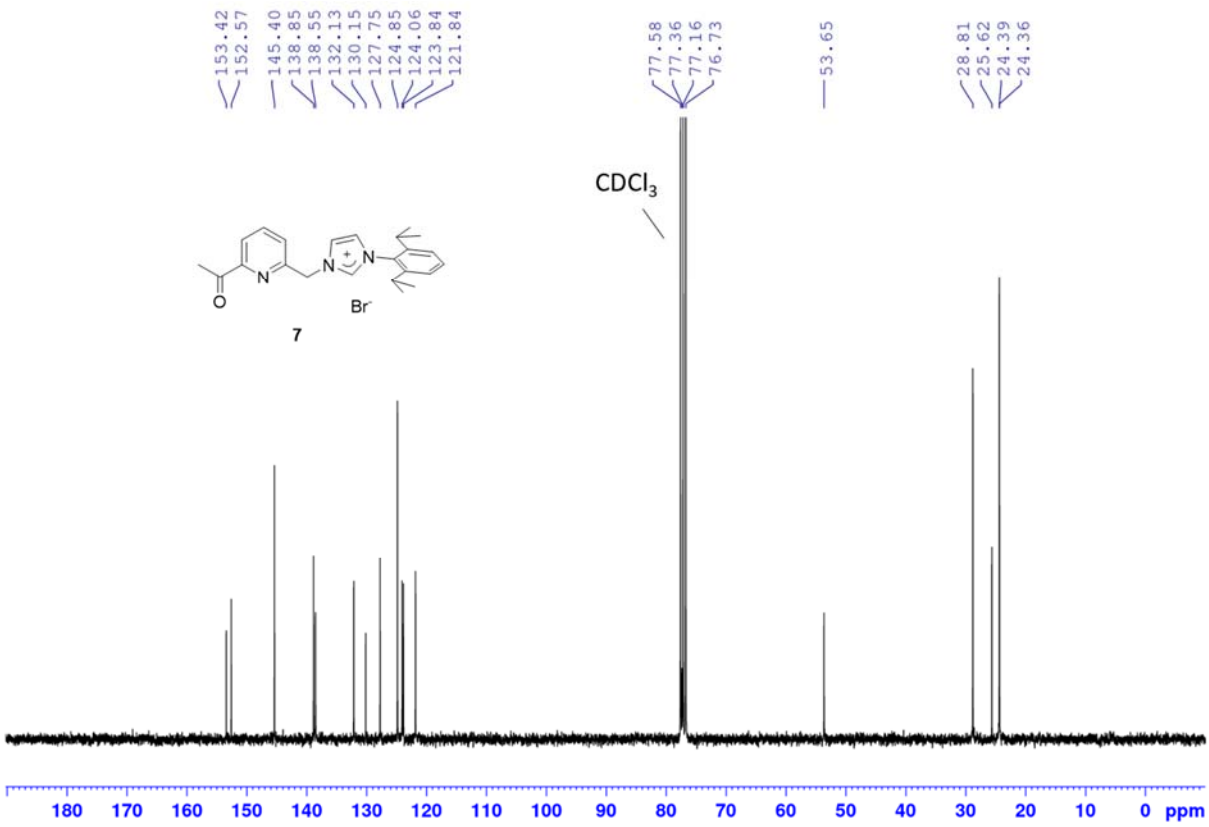

Figure S19. ^{13}C{^{1}H} NMR spectrum of **7** in $CDCl_3$ (solvent signal at δ77.16).

III.5. Compound 8 (L·HBr)

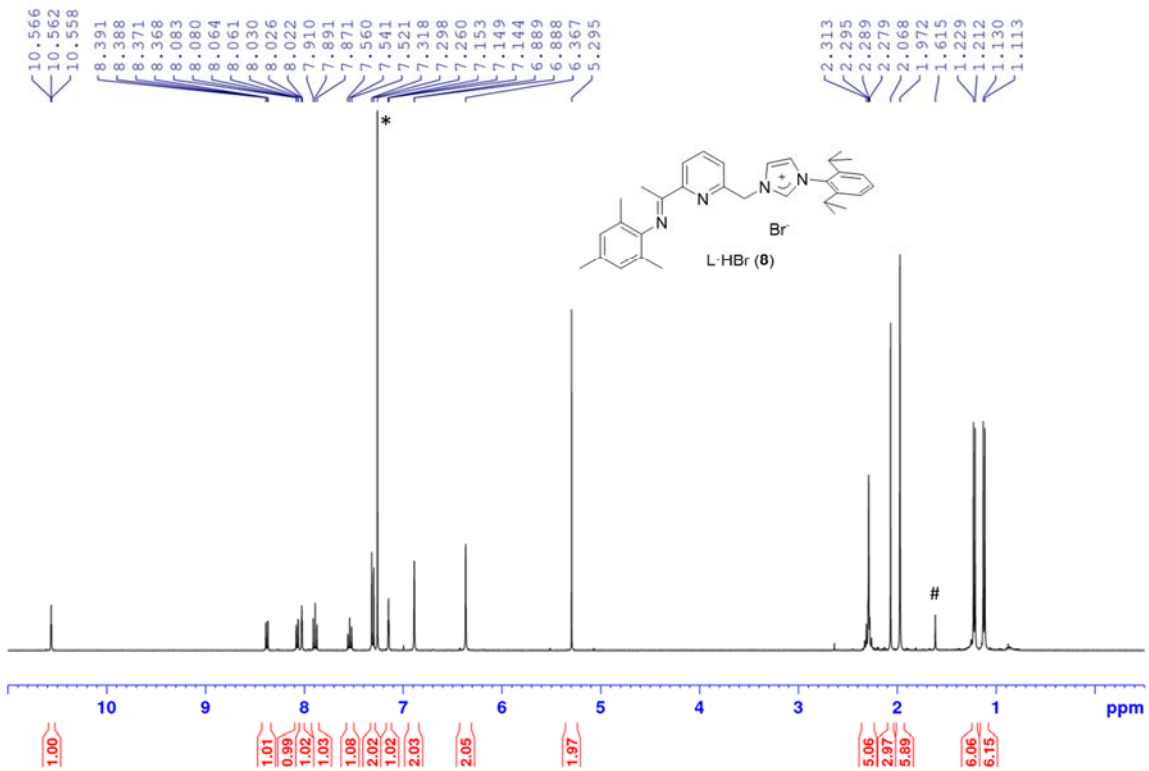

Figure S20. ^{1}H NMR spectrum of L·HBr (**8**) in $CDCl_3$ (residual protio solvent from $CDCl_3$ at δ 7.26 (*)). Traces of an unidentified impurity can be detected at δ 1.62 (#).

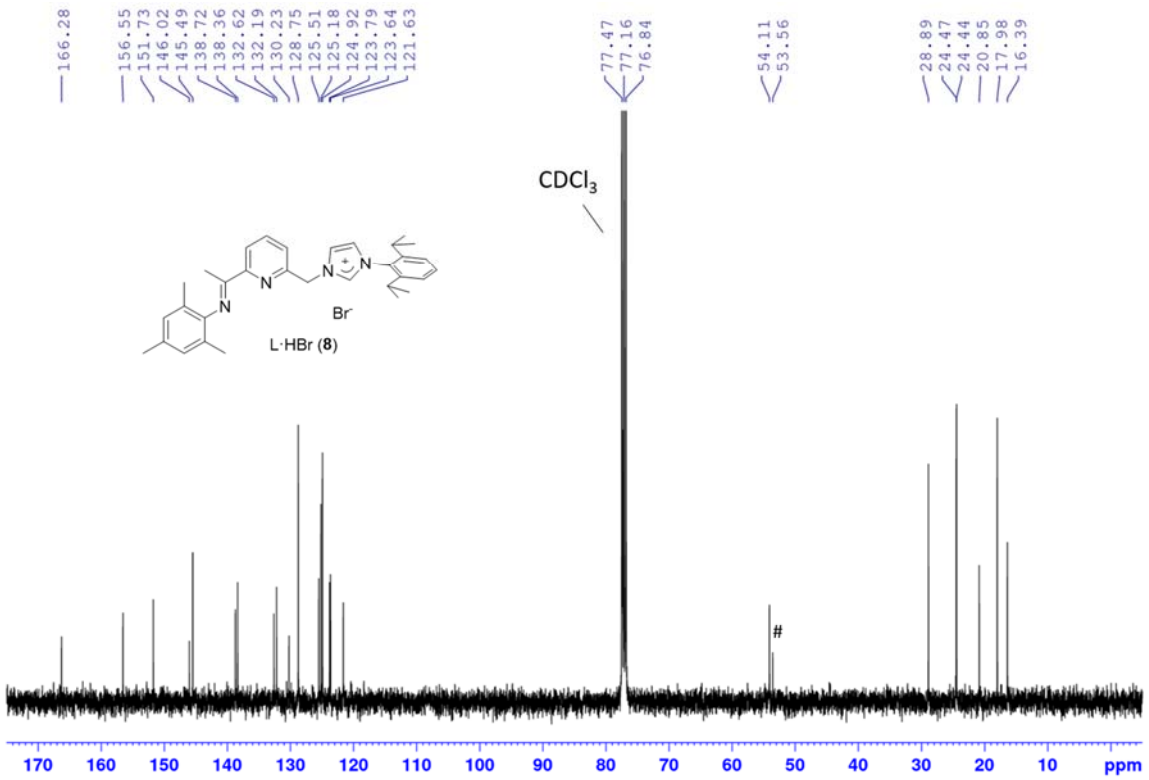

Figure S21. ^{13}C{^{1}H} NMR spectrum of L·HBr (**8**) in $CDCl_3$ (solvent signal at δ 77.16). Traces of an unidentified impurity can be detected at δ 53.6 (#).

III.6. Complex 9

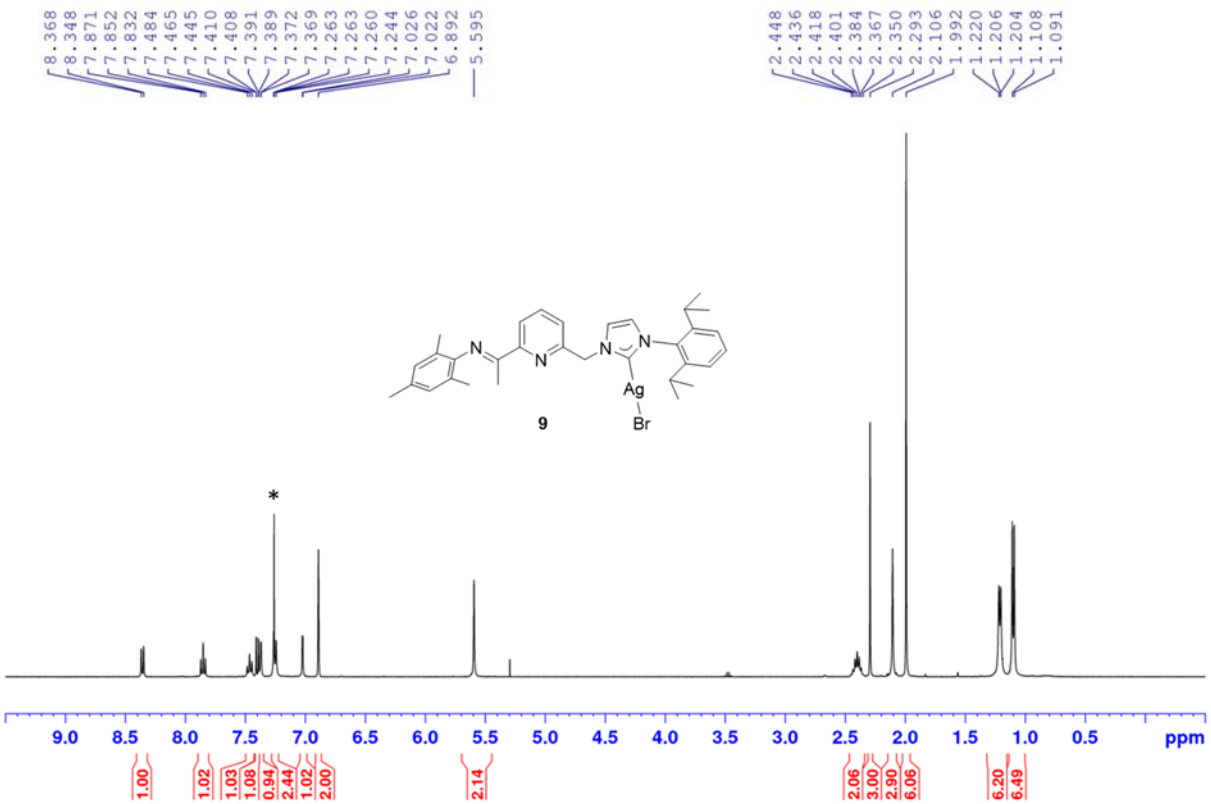

Figure S22. ^{1}H NMR spectrum of **9** in $CDCl_3$ (residual protio solvent from $CDCl_3$ at δ7.26 (*)).

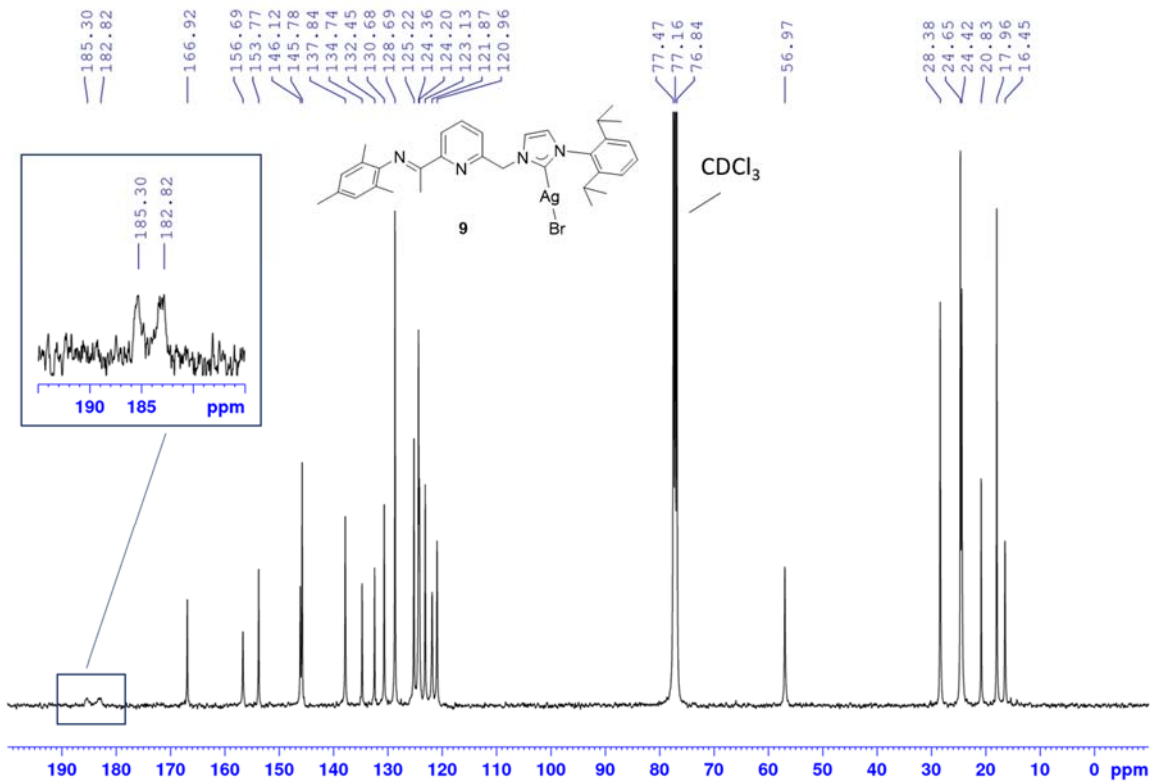

Figure S23. ^{13}C{^{1}H} NMR spectrum of **9** in $CDCl_3$ (solvent signal at δ77.16) at room temperature (298 K). Accumulation of 10 000 scans with a sample at high concentration (*ca*. 60 mg.mL^{-1}).

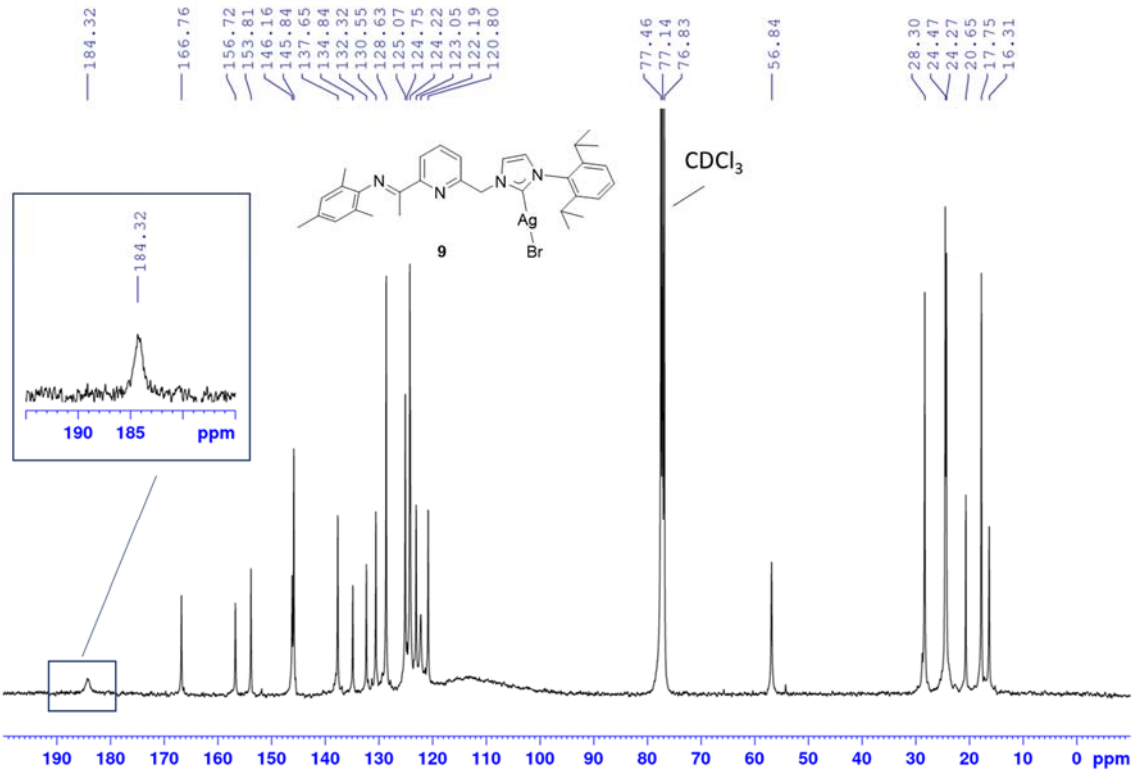

Figure S24. $^{13}C\{^{1}H\}$ NMR spectrum of **9** in $CDCl_3$ (solvent signal at δ77.14) at high temperature (323 K). Accumulation of *ca*. 11 500 scans with a sample at high concentration (*ca*. 120 mg.mL^{-1}).

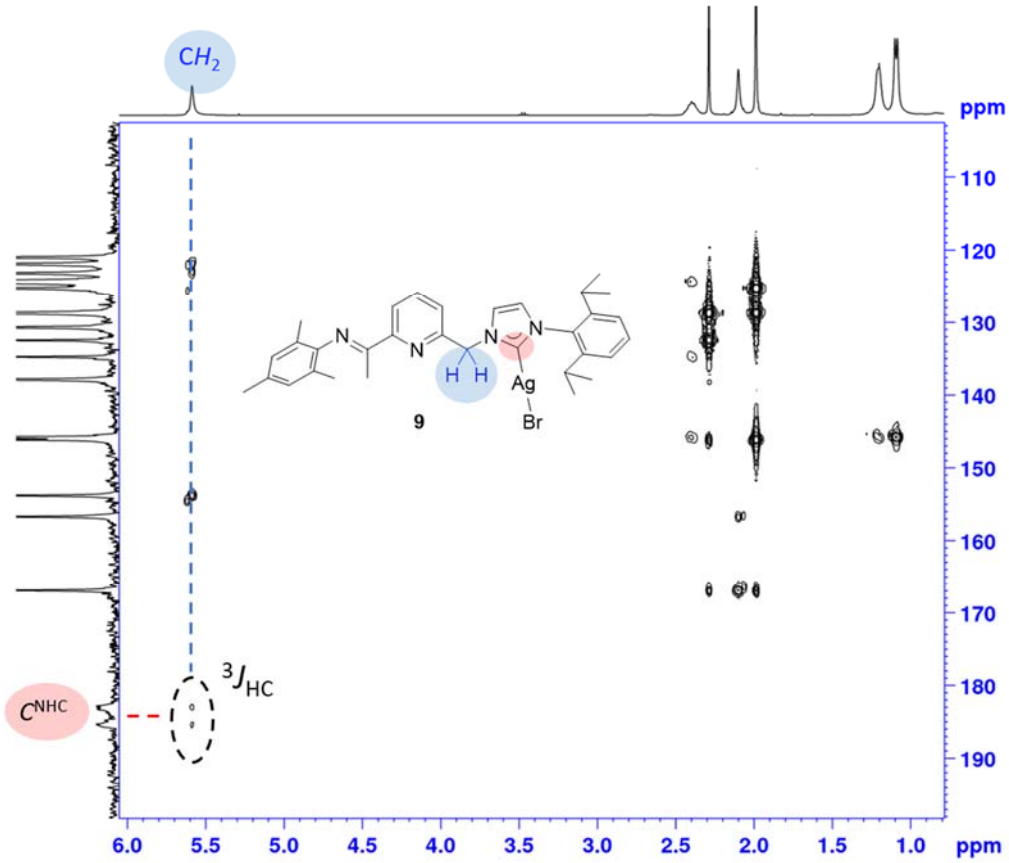

Figure S25. Detail of the ^{1}H-^{13}C HMBC spectrum of **9** at room temperature (298 K) confirming the assignment of the C^{NHC} resonance.

III.7. Complex 10

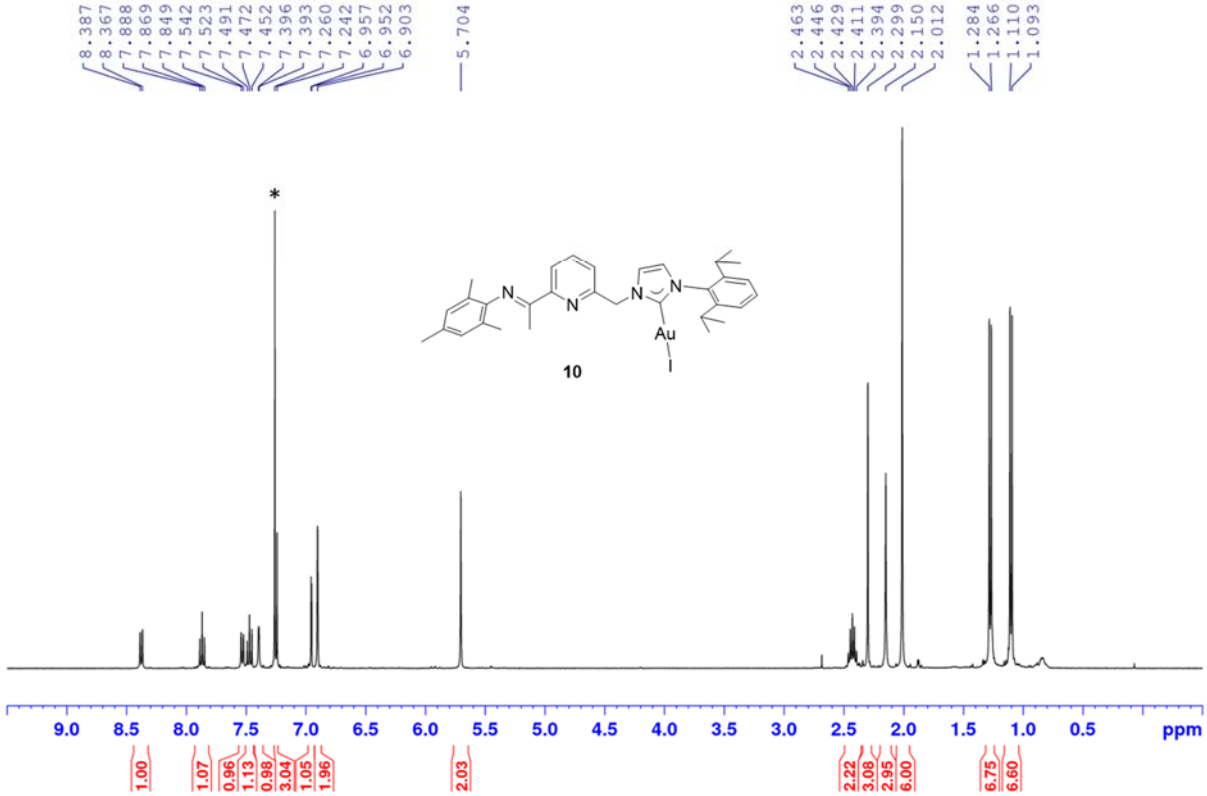

Figure S26. ^{1}H NMR spectrum of **10** in $CDCl_3$ (residual protio solvent from $CDCl_3$ at δ7.26 (*)).

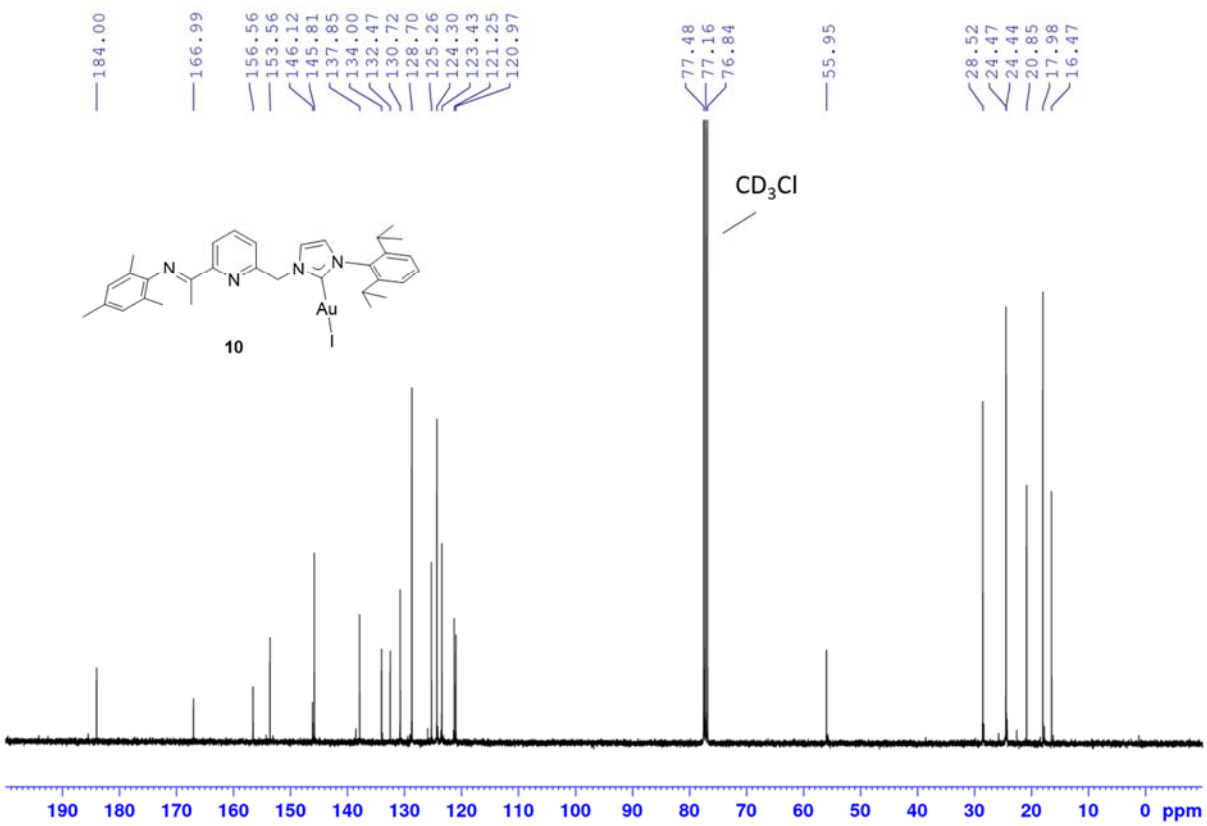

Figure S27. ^{13}C{^{1}H} NMR spectrum of **10** in $CDCl_3$ (solvent signal at δ77.16).

III.8. Complex 11

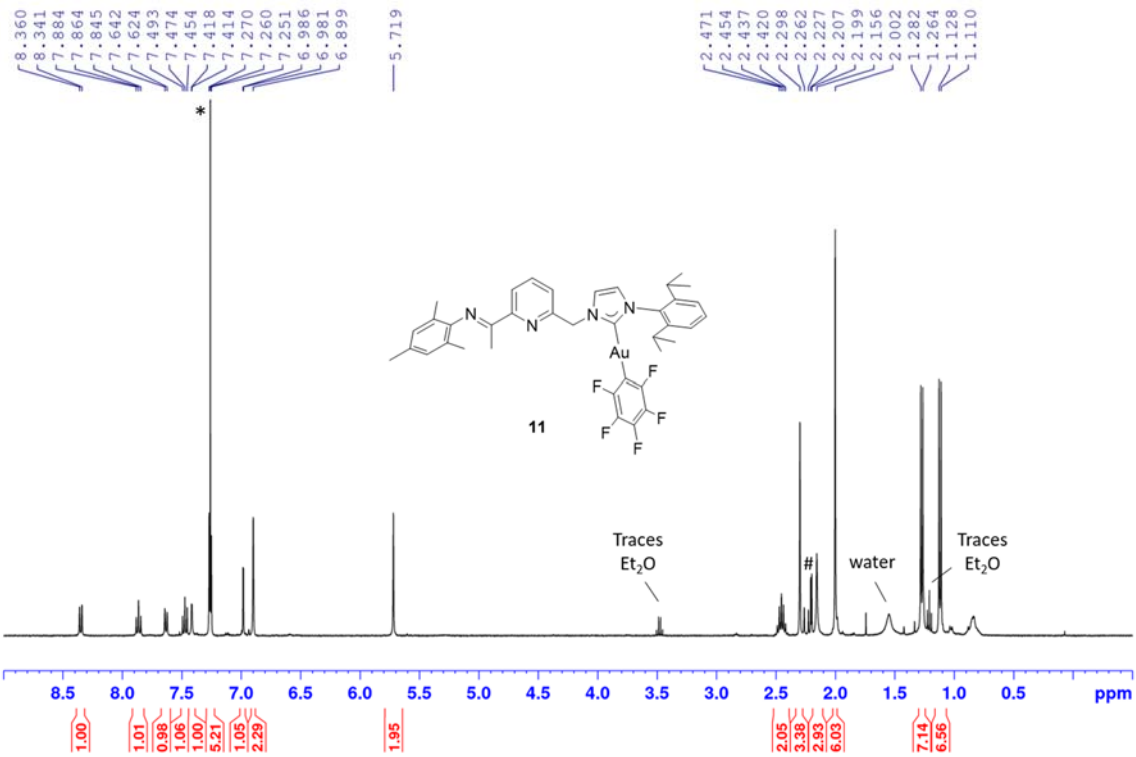

Figure S28. ^{1}H NMR spectrum of **11** in $CDCl_3$ (residual protio solvent from $CDCl_3$ at δ7.26 (*)). Traces of water (δ1.56), Et_2O (δ3.48 and 1.21) and an unidentified impurity (#, δ2.20) can be detected.

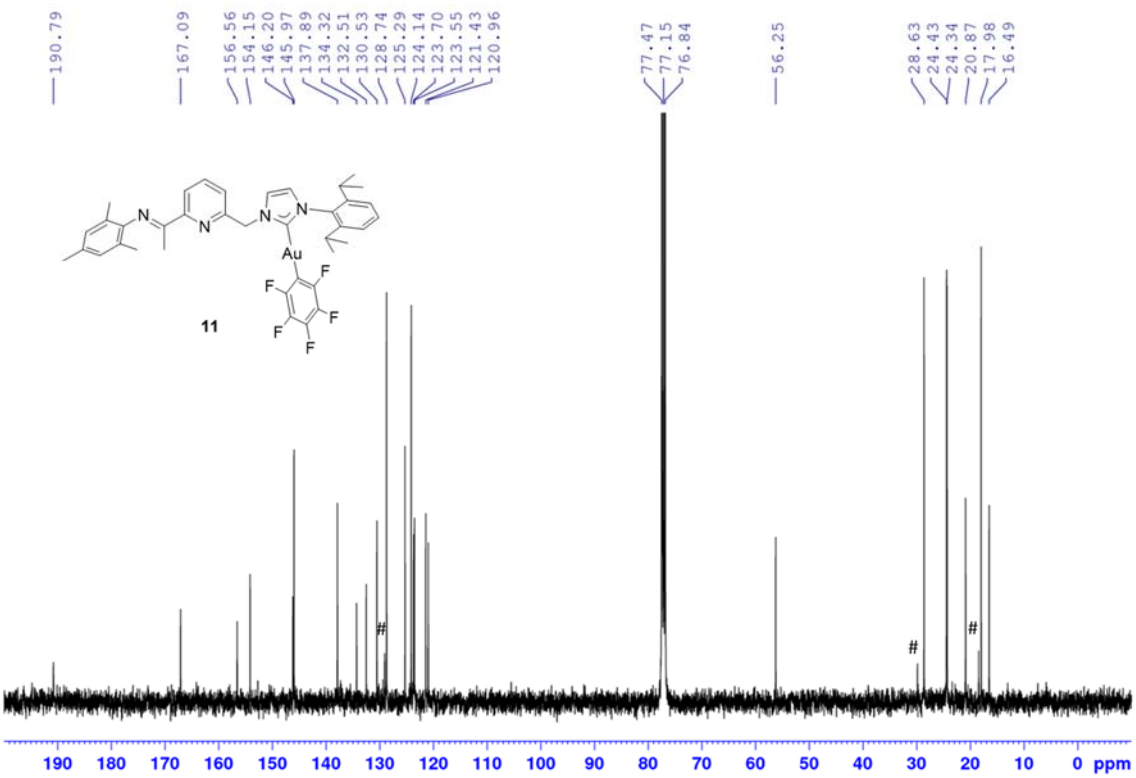

Figure S29. ^{13}C{^{1}H} NMR spectrum of **11** in $CDCl_3$ (solvent signal at δ77.16). Traces of an unidentified impurity (#) can be detected at δ129.1, 29.9 and 18.5.

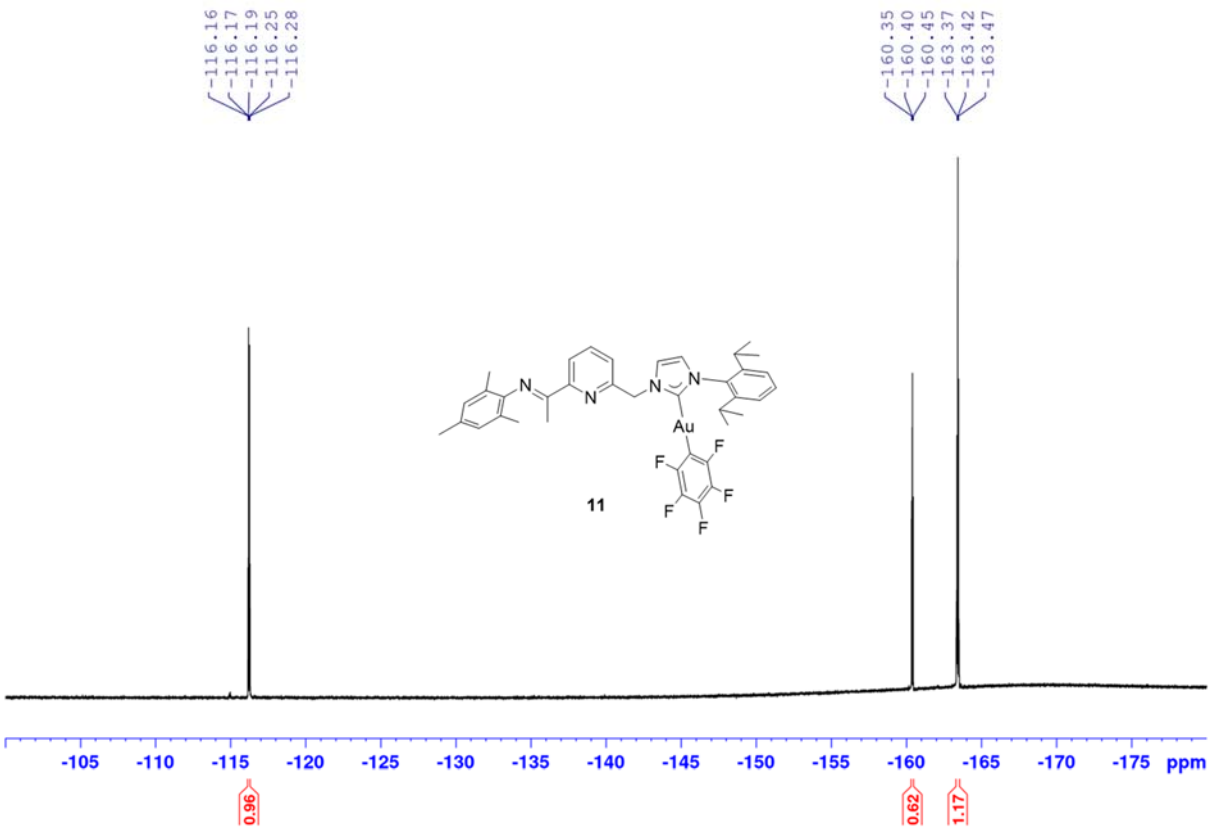

Figure S30. ^{19}F NMR spectrum of **11** in $CDCl_3$.

III.9. Complex 12

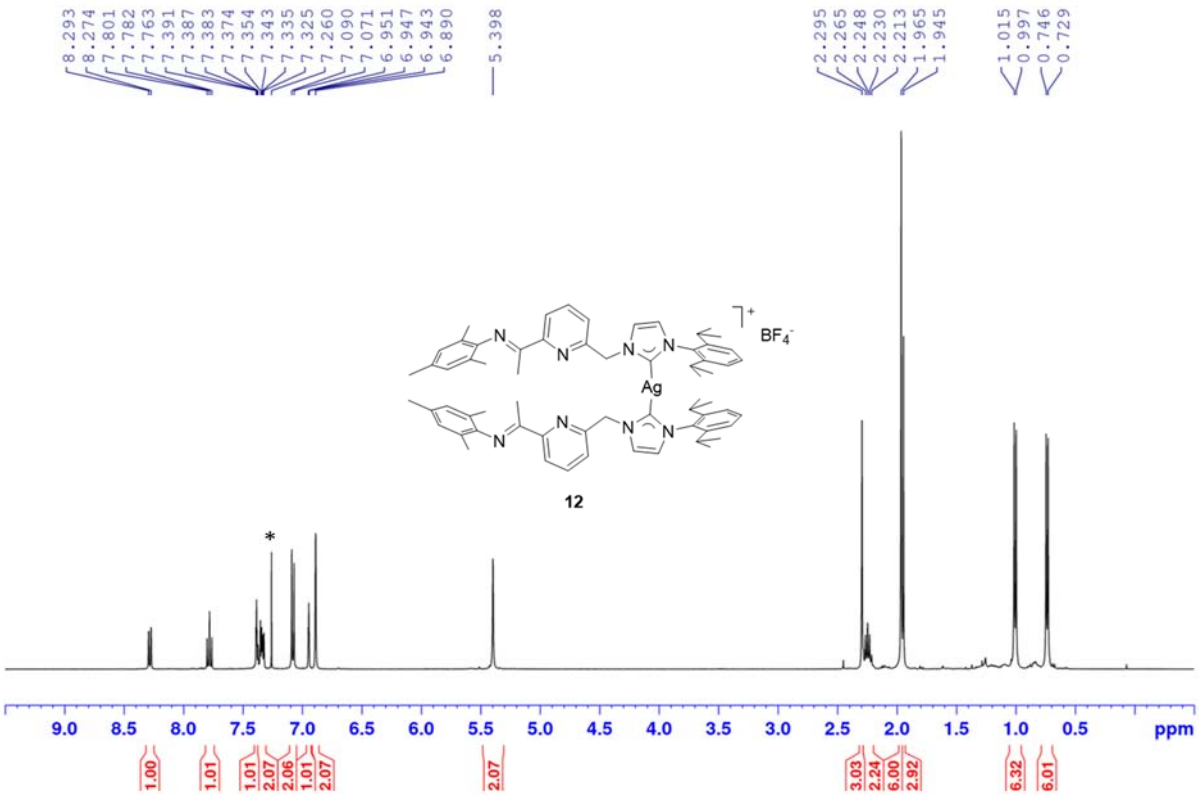

Figure S31. ^{1}H NMR spectrum of **12** in $CDCl_3$ (residual protio solvent from $CDCl_3$ at δ7.26 (*)).

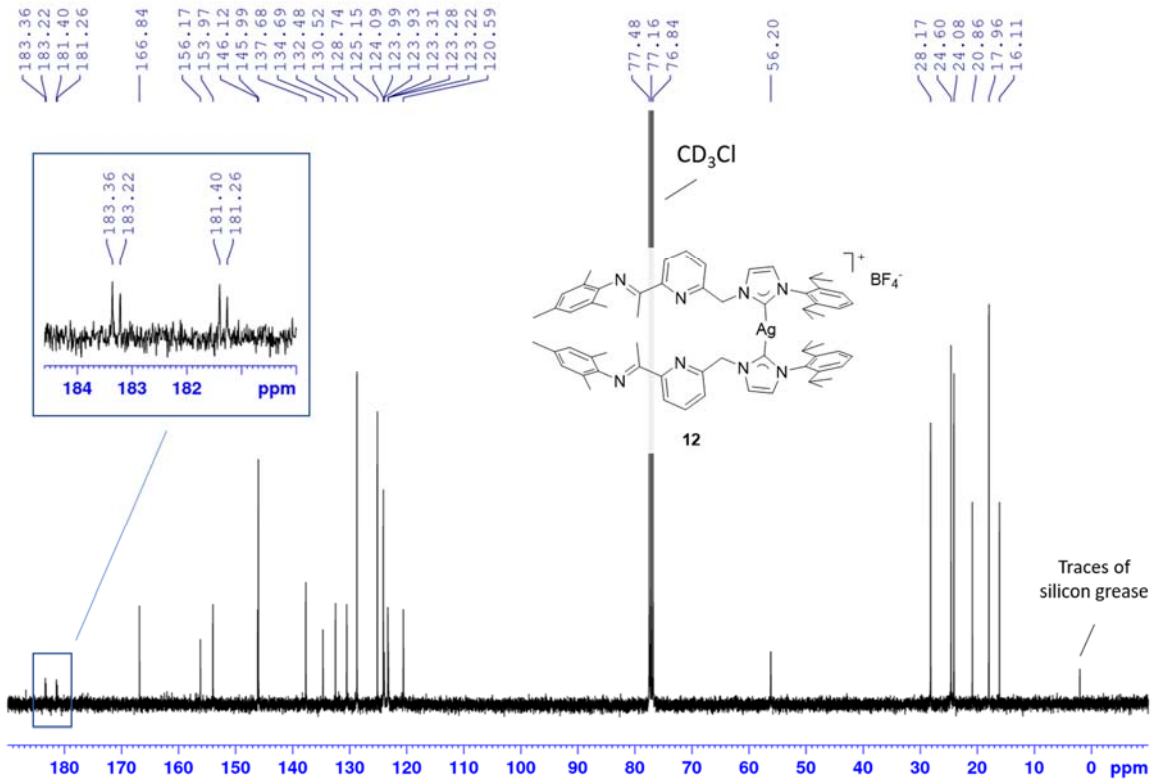

Figure S32. $^{13}C\{^1H\}$ NMR spectrum of **12** in $CDCl_3$ (solvent signal at δ77.16). Traces of silicon grease can be detected at δ2.0.

III.10. Complex 13

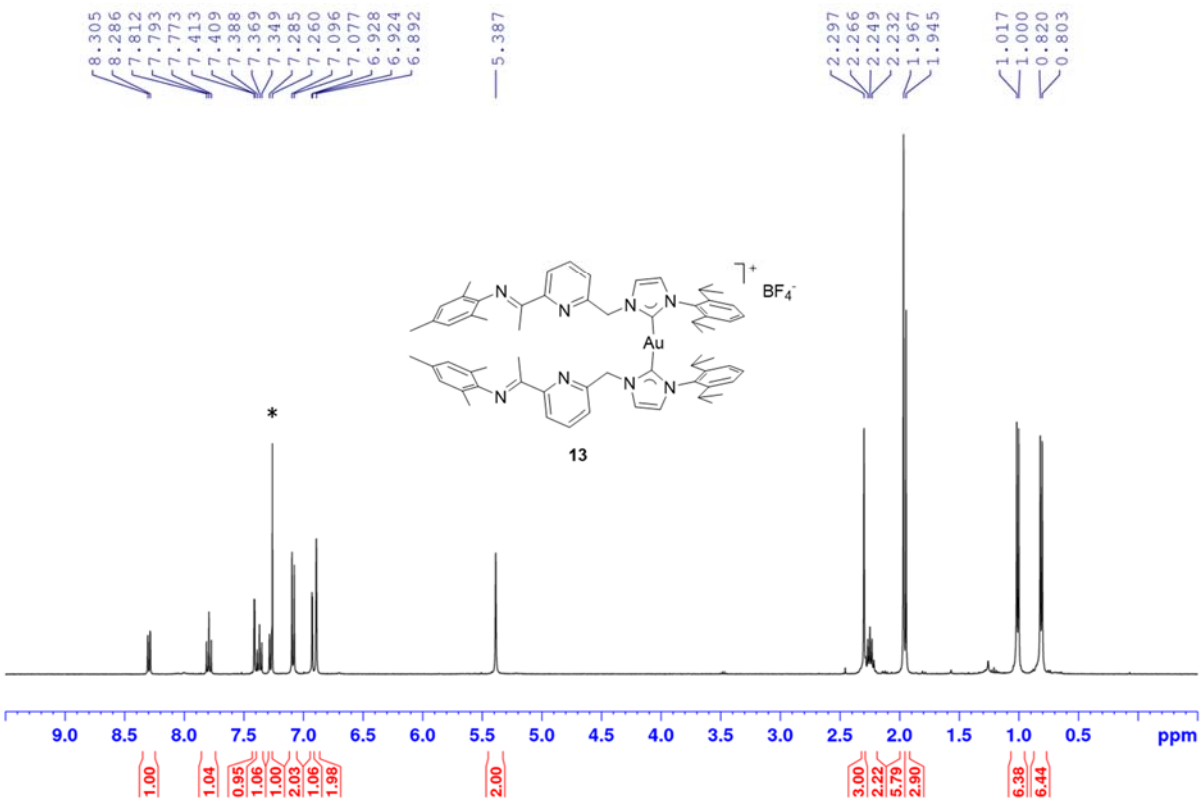

Figure S33. ^1H NMR spectrum of **13** in $CDCl_3$ (residual protio solvent from $CDCl_3$ at δ7.26 (*)).

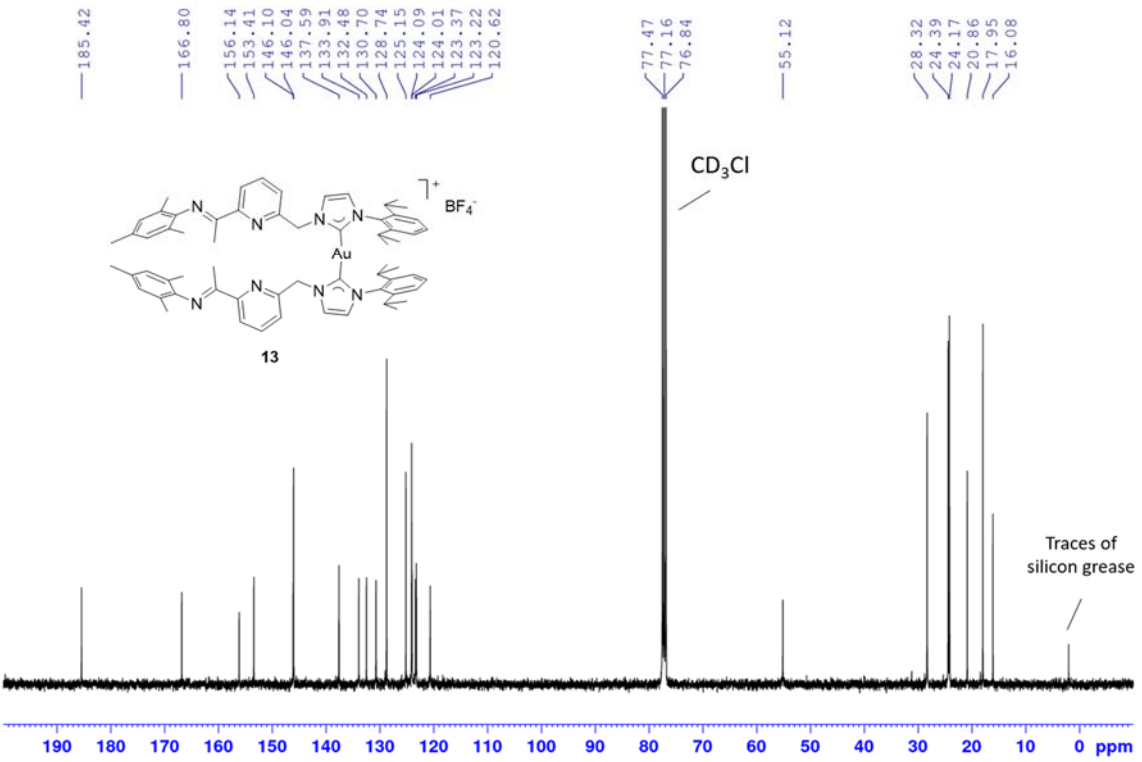

Figure S34. $^{13}C\{^{1}H\}$ NMR spectrum of **13** in $CDCl_3$ (solvent signal at δ77.16). Traces of silicon grease can be detected at δ2.0.

III.11. Complex 14

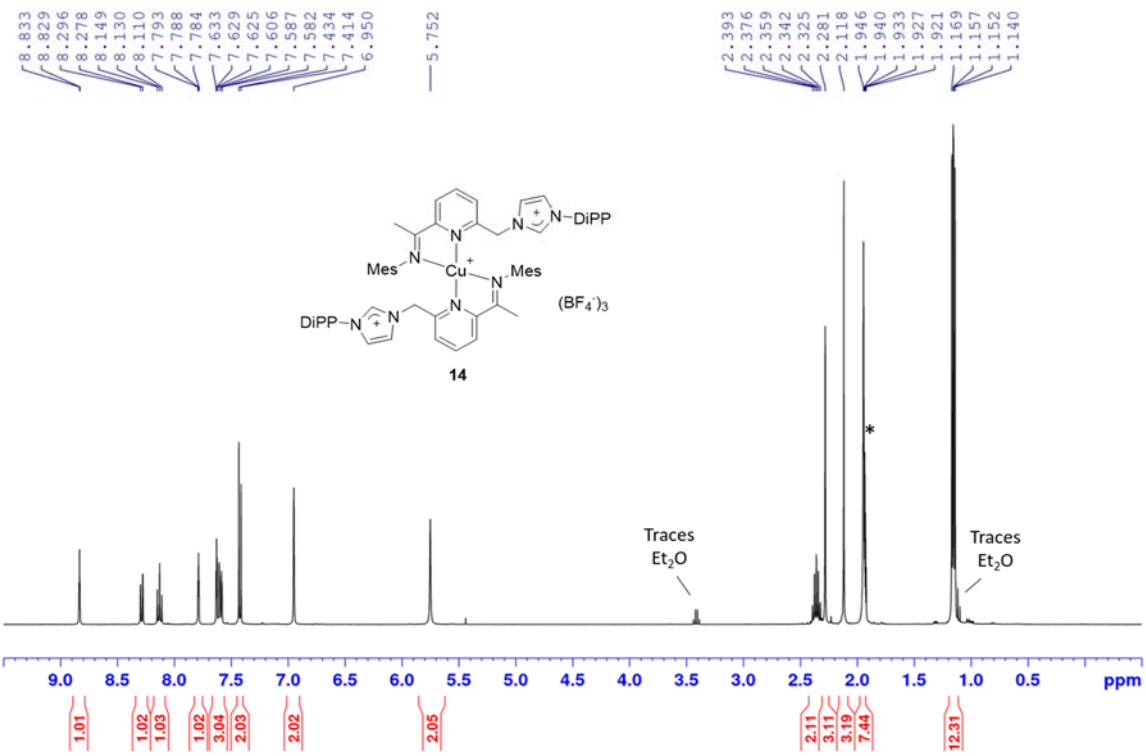

Figure S35. ^{1}H NMR spectrum of **14** in CD_3CN (residual protio solvent from CD_3CN at δ1.94 (*)). Traces of Et_2O can be detected at δ3.42 and 1.12.

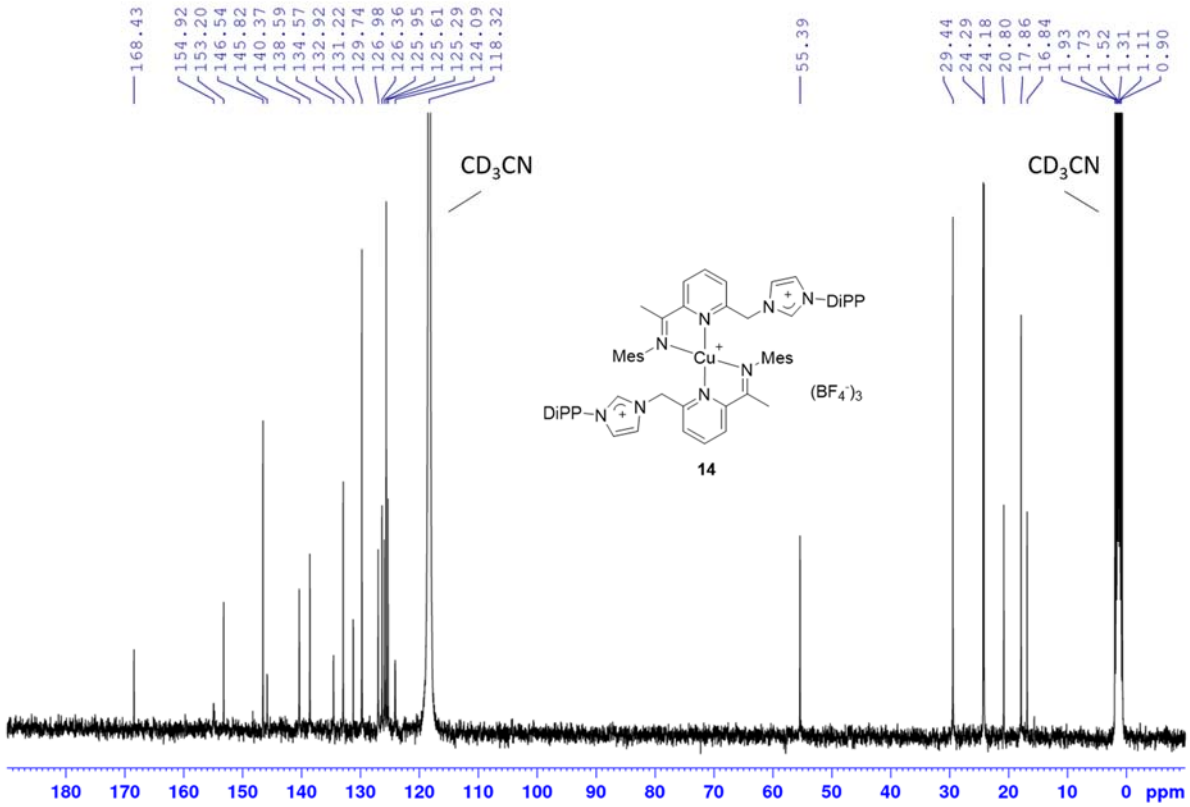

Figure S36. $^{13}C\{^{1}H\}$ NMR spectrum of **14** in CD_3CN (solvent signal at δ118.32 and 1.31).

III.12. Complex 15

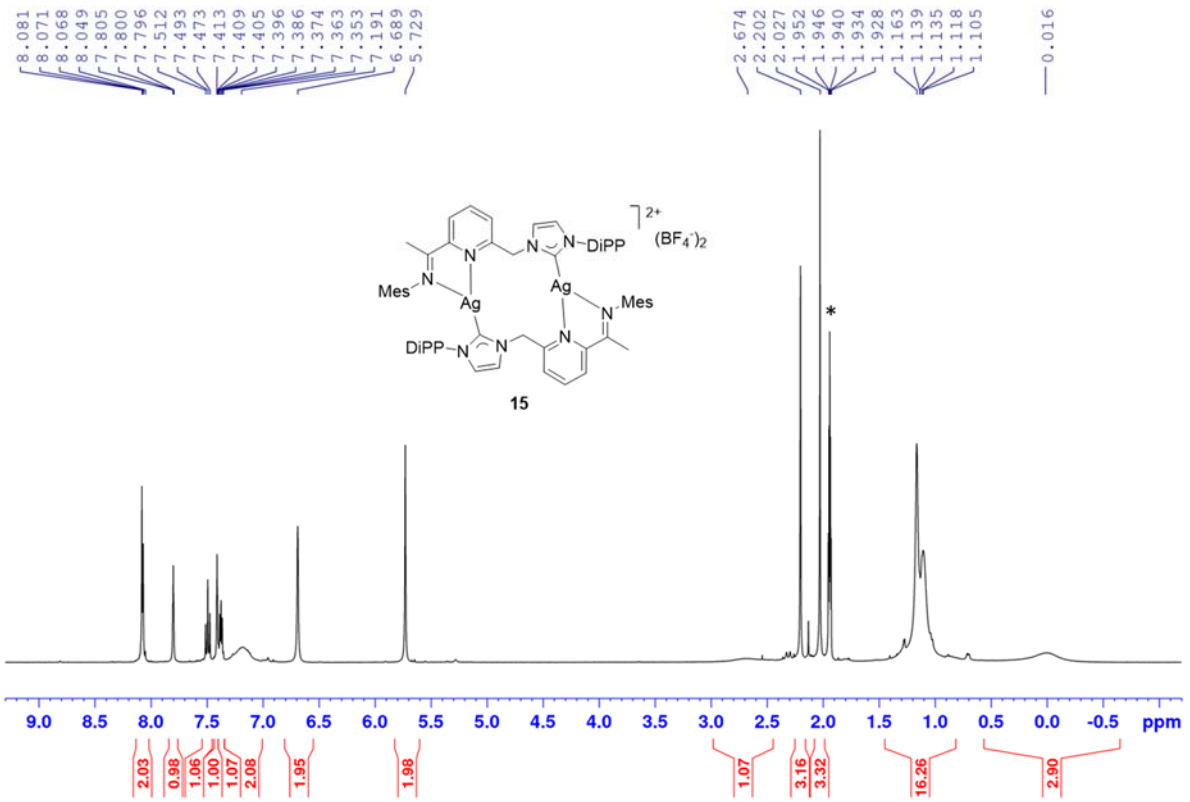

Figure S37. ^{1}H NMR spectrum of **15** in CD_3CN (residual protio solvent from CD_3CN at δ1.94 (*)).

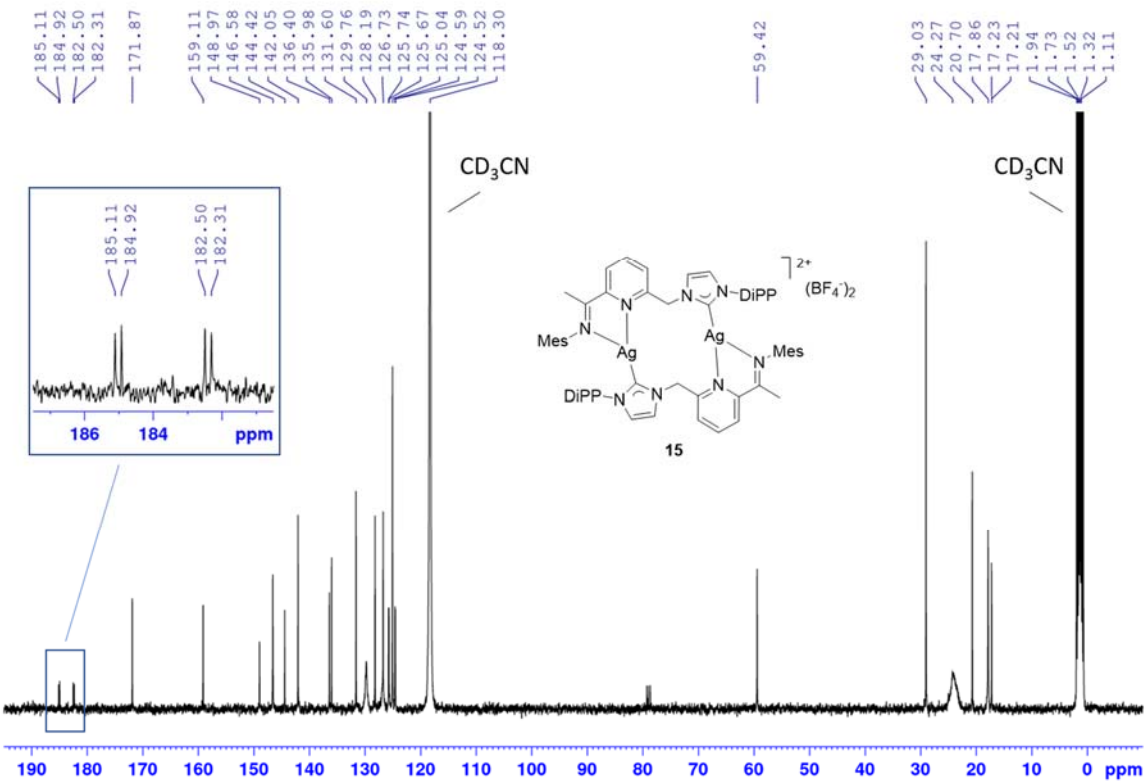

Figure S38. $^{13}C\{^{1}H\}$ NMR spectrum of **15** in CD_3CN (solvent signal at δ118.30 and 1.32).

III.13. Complex 16

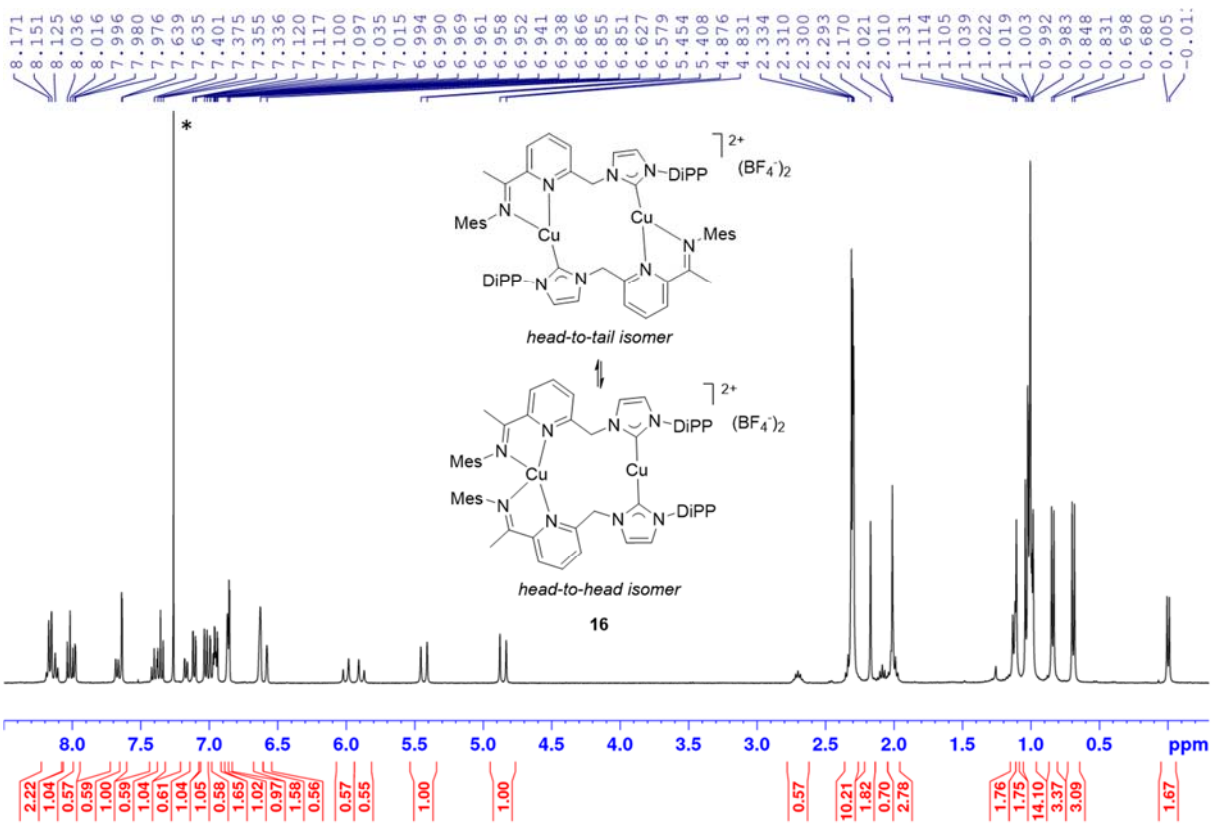

Figure S39. ^{1}H NMR spectrum of **16** in $CDCl_3$ (residual protio solvent from $CDCl_3$ at δ7.26 (*)).

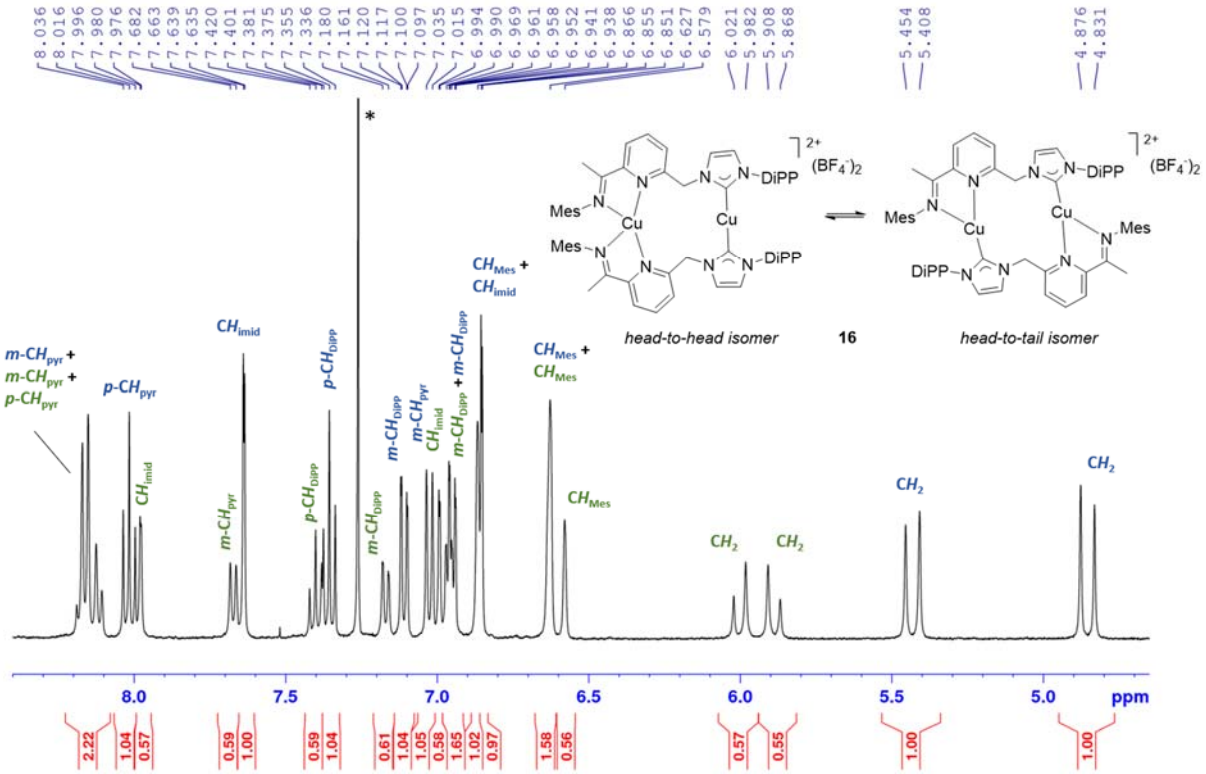

Figure S40. Detail of the ^{1}H NMR spectrum of **16** in $CDCl_3$ in the region δ8.5–4.5 (residual protio solvent from $CDCl_3$ at δ7.26 (*)) and assignment of the signals corresponding to the two isomers.

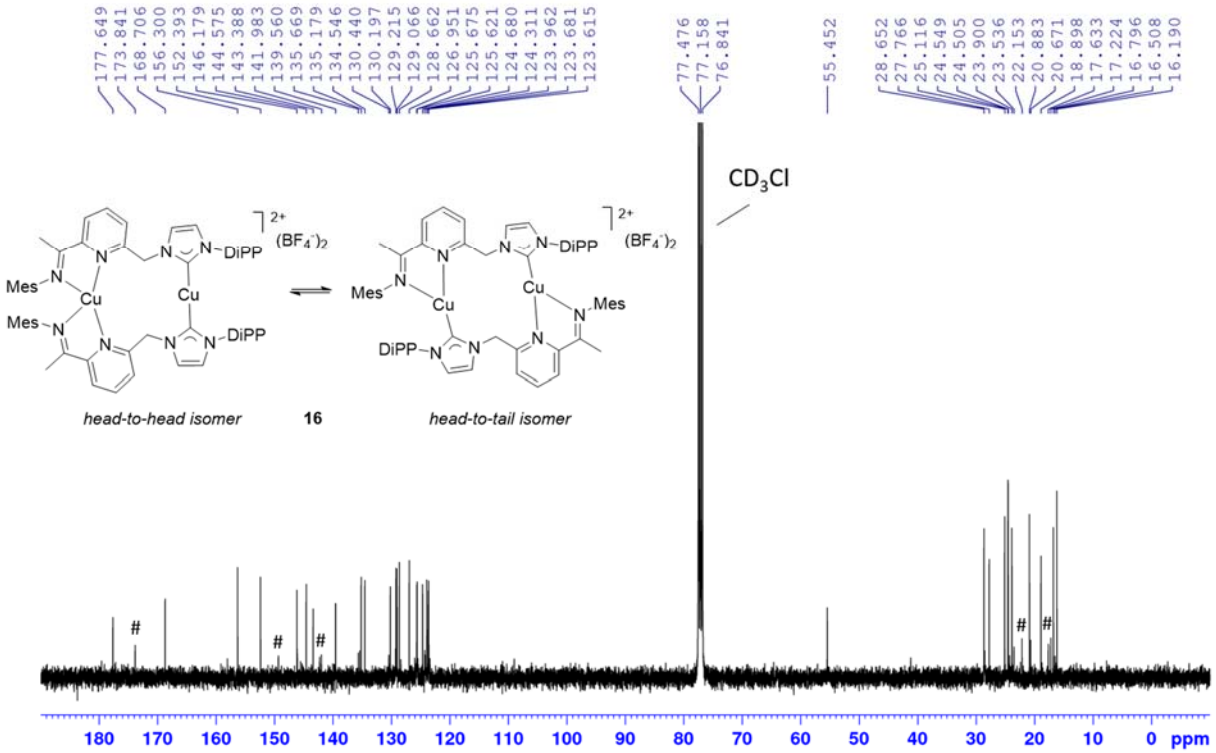

Figure S41. ^{13}C{^{1}H} NMR spectrum of **16** in $CDCl_3$ (solvent signal at δ77.16). The label # corresponds to signals arising from the minor isomer.

III.14. Complex 17

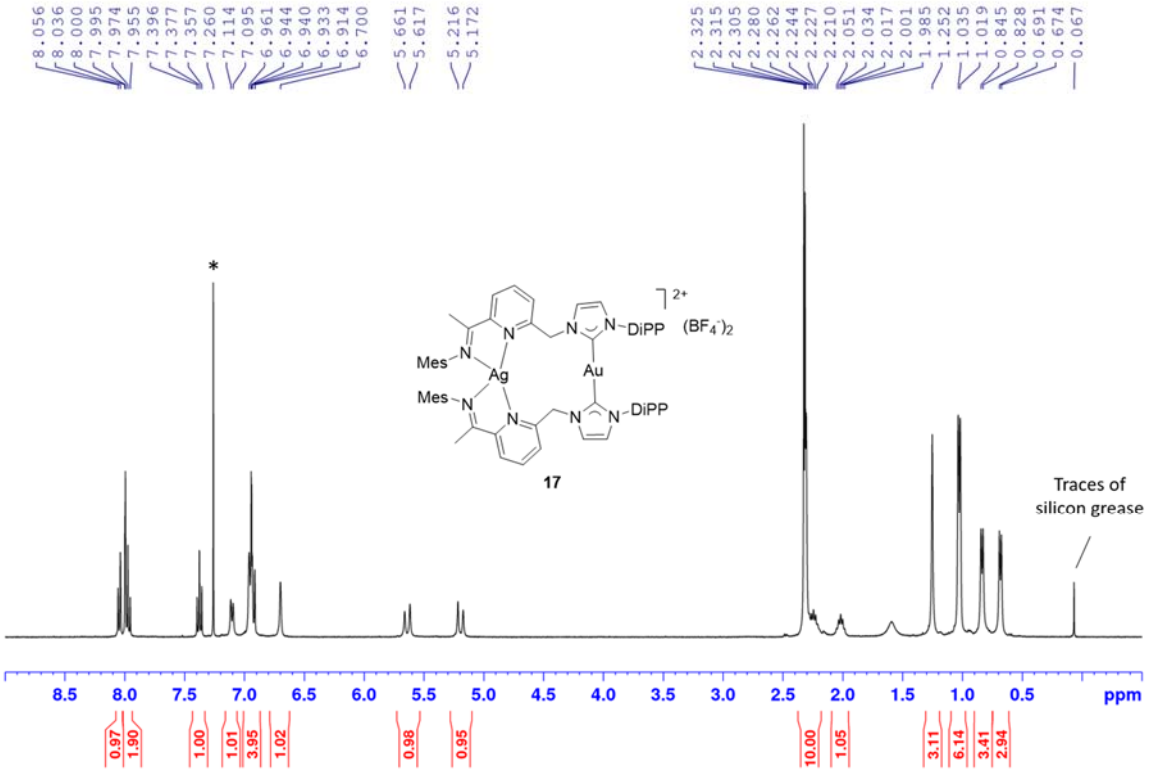

Figure S42. ^{1}H NMR spectrum of **17** in $CDCl_3$ (residual protio solvent from $CDCl_3$ at δ7.26 (*)). Traces of silicon grease can be detected at δ0.07.

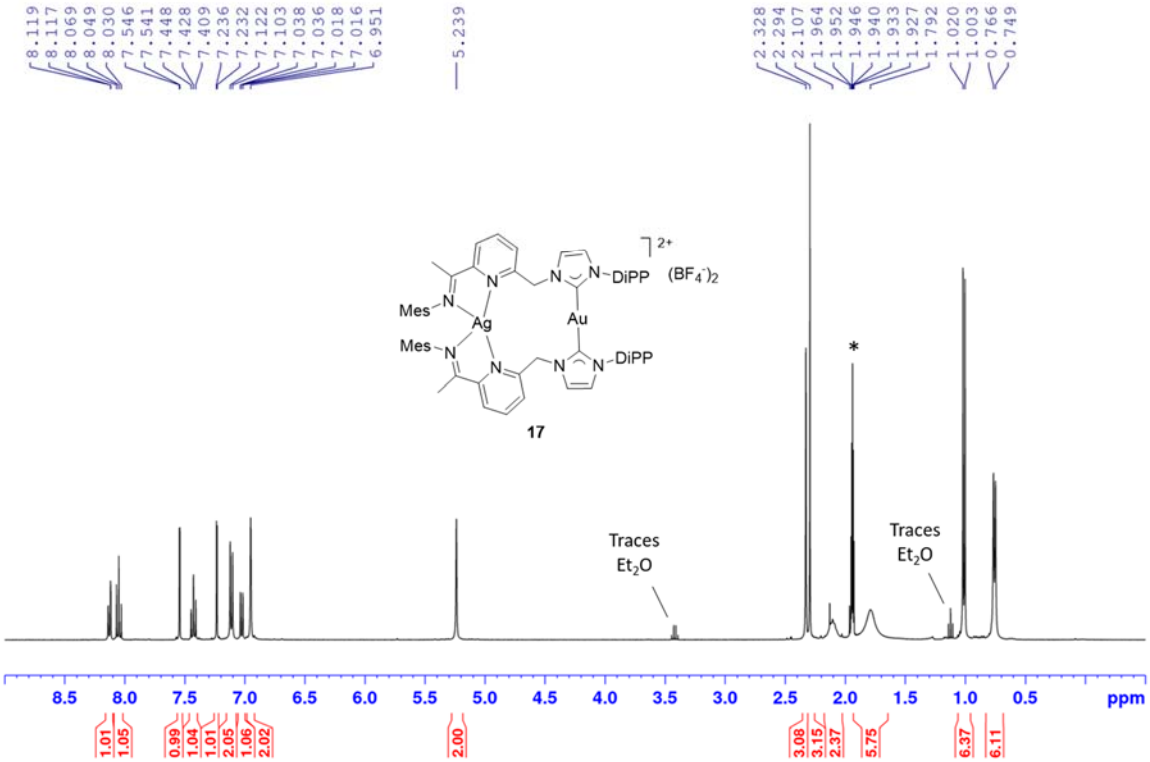

Figure S43. ^{1}H NMR spectrum of **17** in CD_3CN (residual protio solvent from CD_3CN at δ1.94 (*)). Traces of Et_2O can be detected at δ3.42 and 1.12.

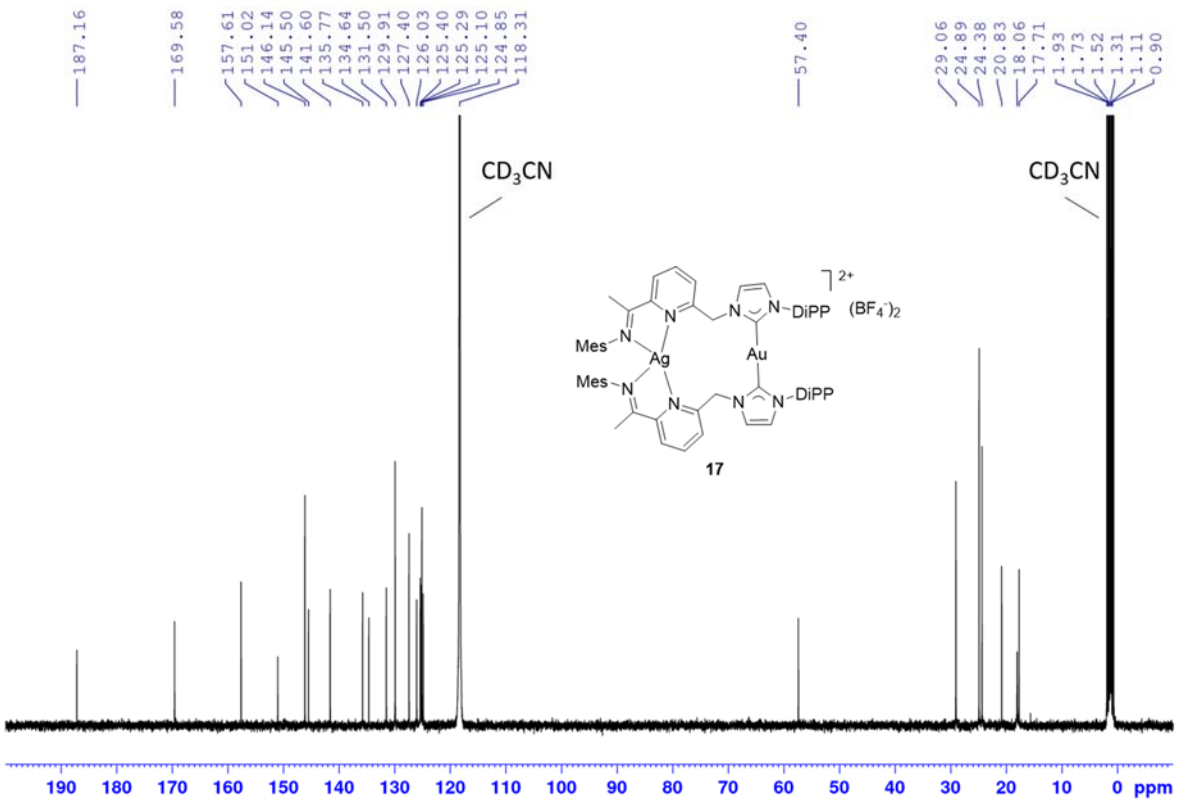

Figure S44. $^{13}C\{^{1}H\}$ NMR spectrum of **17** in CD_3CN (solvent signal at δ118.31 and 1.31).

III.15. Complex 18

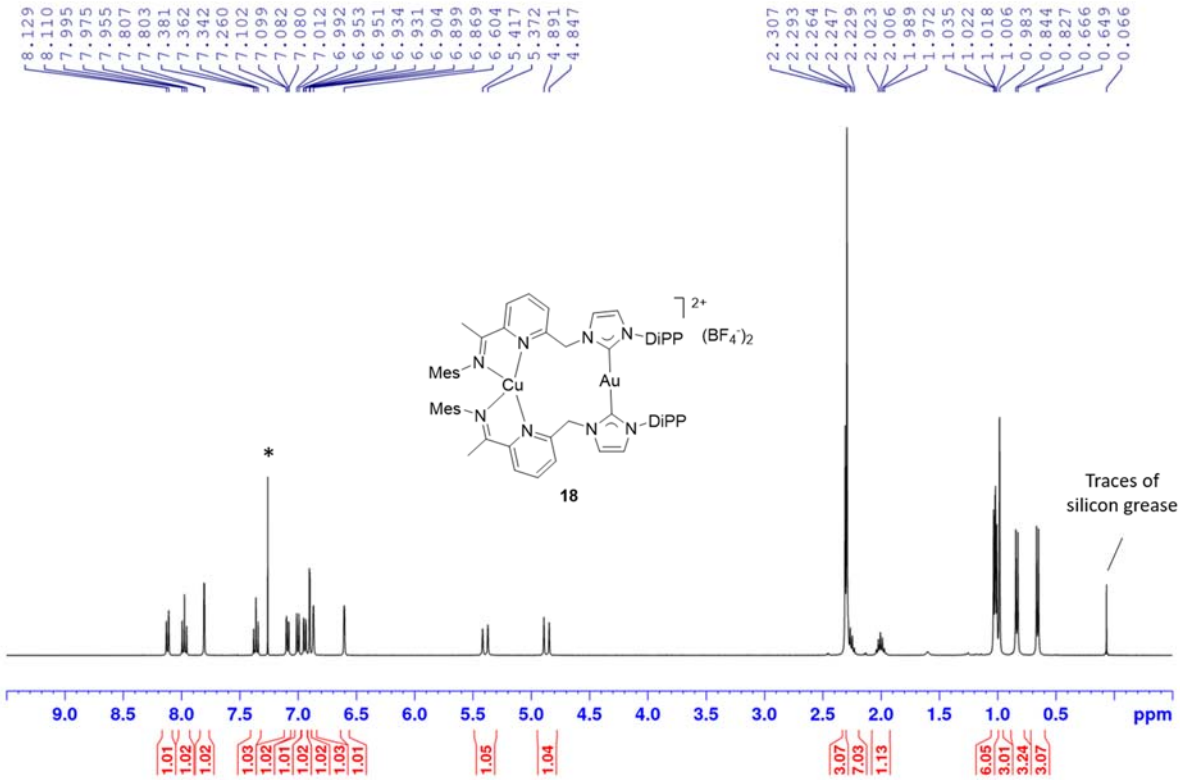

Figure S45. ^{1}H NMR spectrum of **18** in $CDCl_3$ (residual protio solvent from $CDCl_3$ at δ7.26 (*)). Traces of silicon grease can be detected at δ0.07.

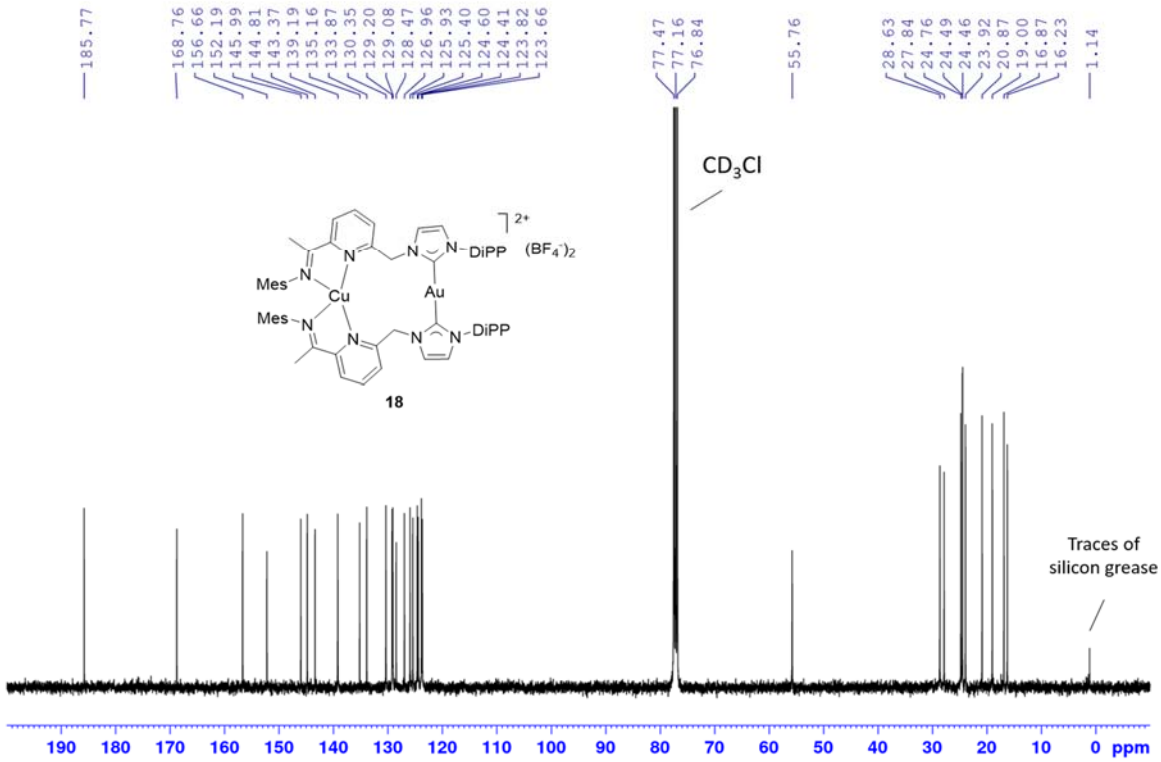

Figure S46. $^{13}C\{^1H\}$ NMR spectrum of **18** in $CDCl_3$ (solvent signal at δ77.16). Traces of silicon grease can be detected at δ1.1.

IV. IR SPECTRA

IV.1. Compound 8 (L·HBr)

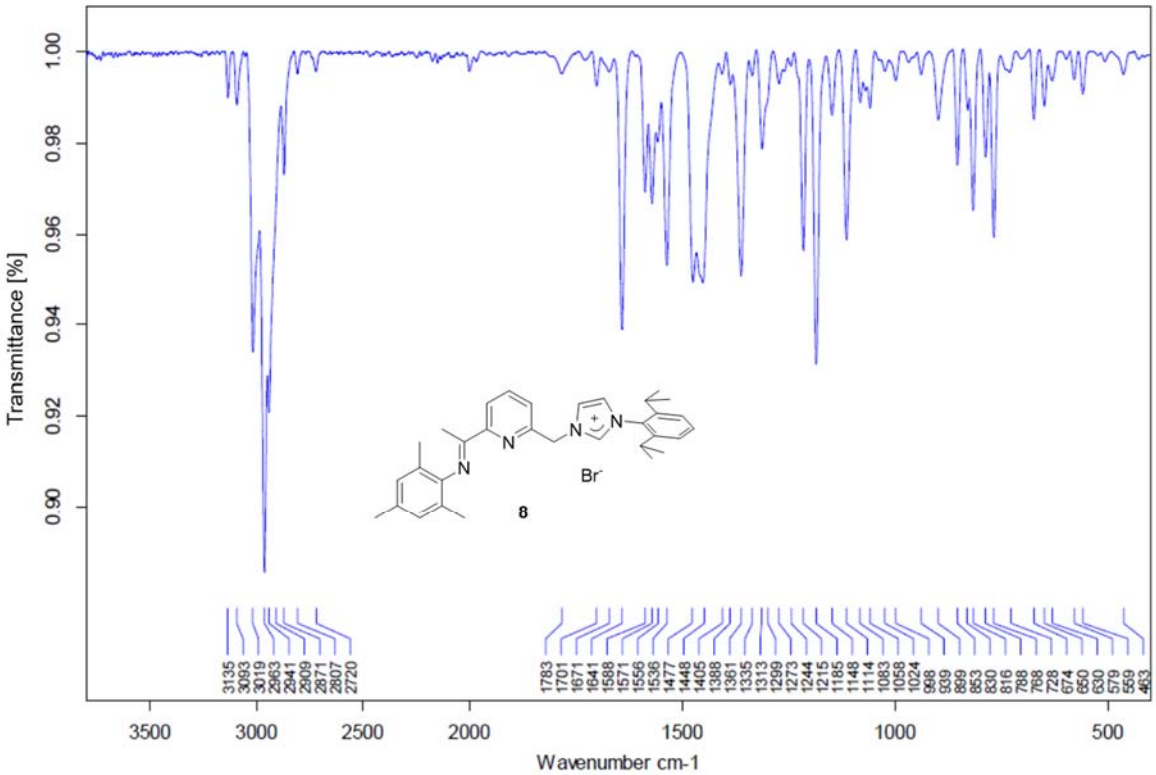

Figure S47. IR spectrum of L·HBr (**8**).

IV.2. Complex 9

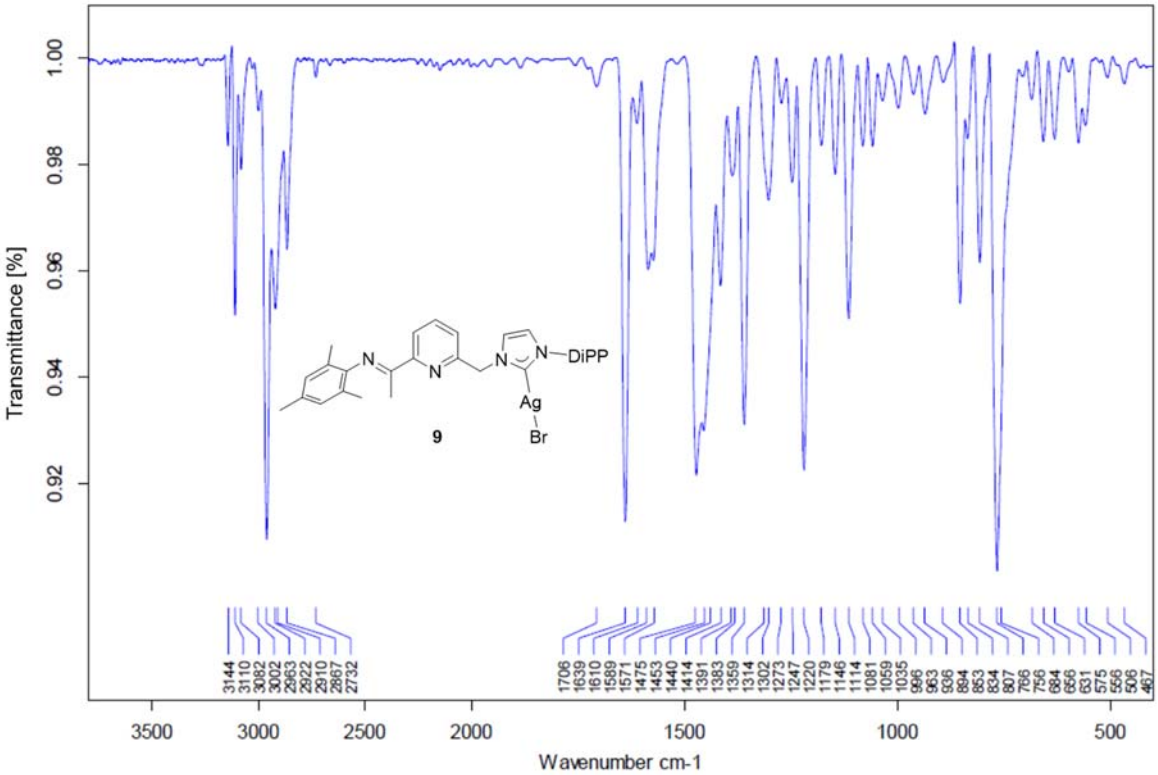

Figure S48. IR spectrum of complex **9**.

IV.3. Complex 10

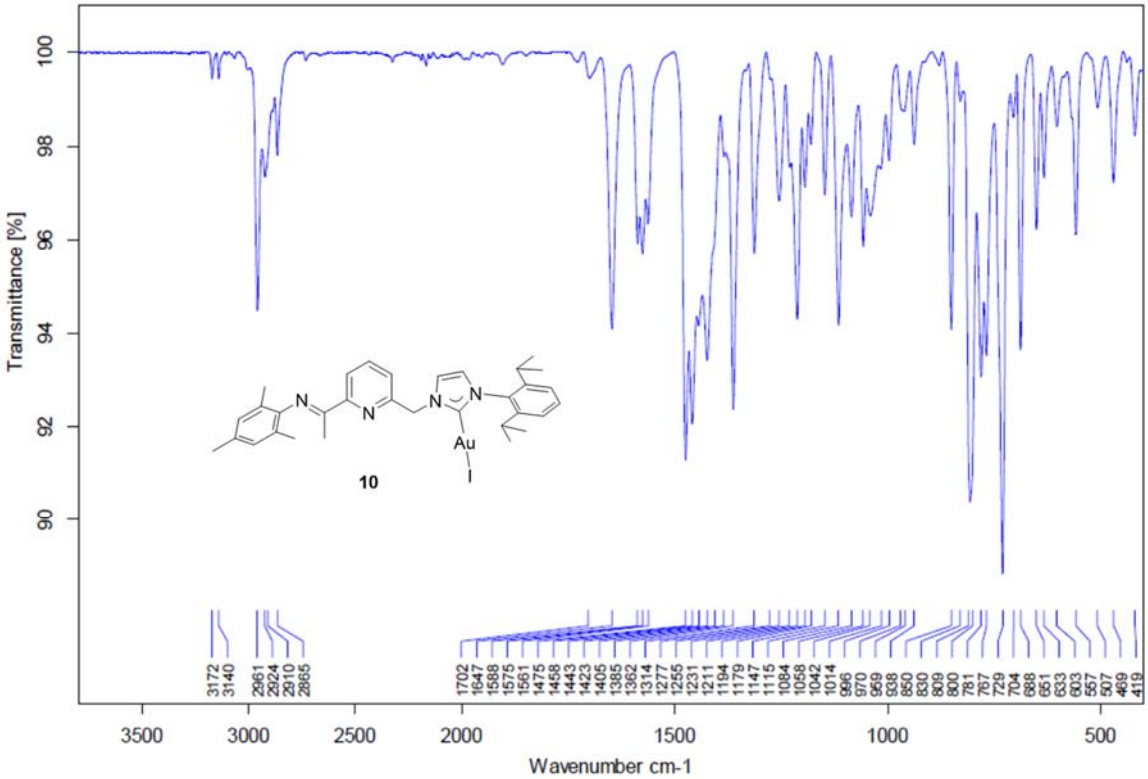

Figure S49. IR spectrum of complex **10**.

IV.4. Complex 11

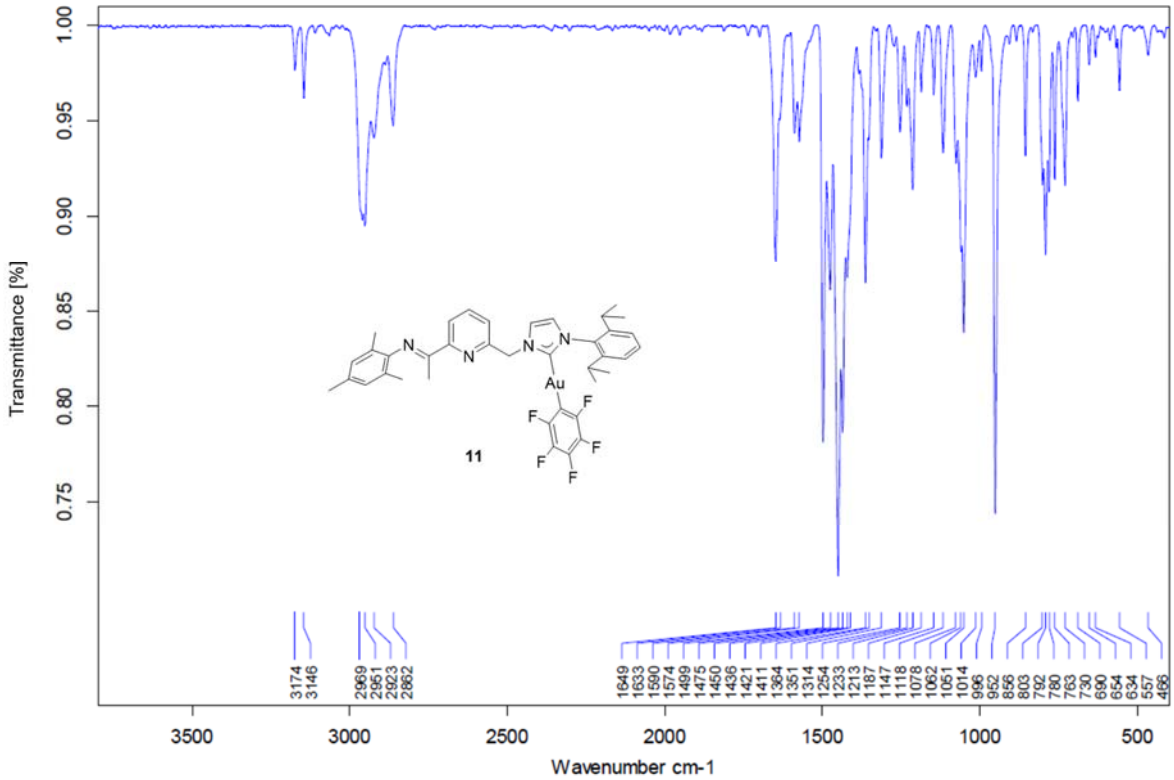

Figure S50. IR spectrum of complex **11**.

IV.5. Complex 12

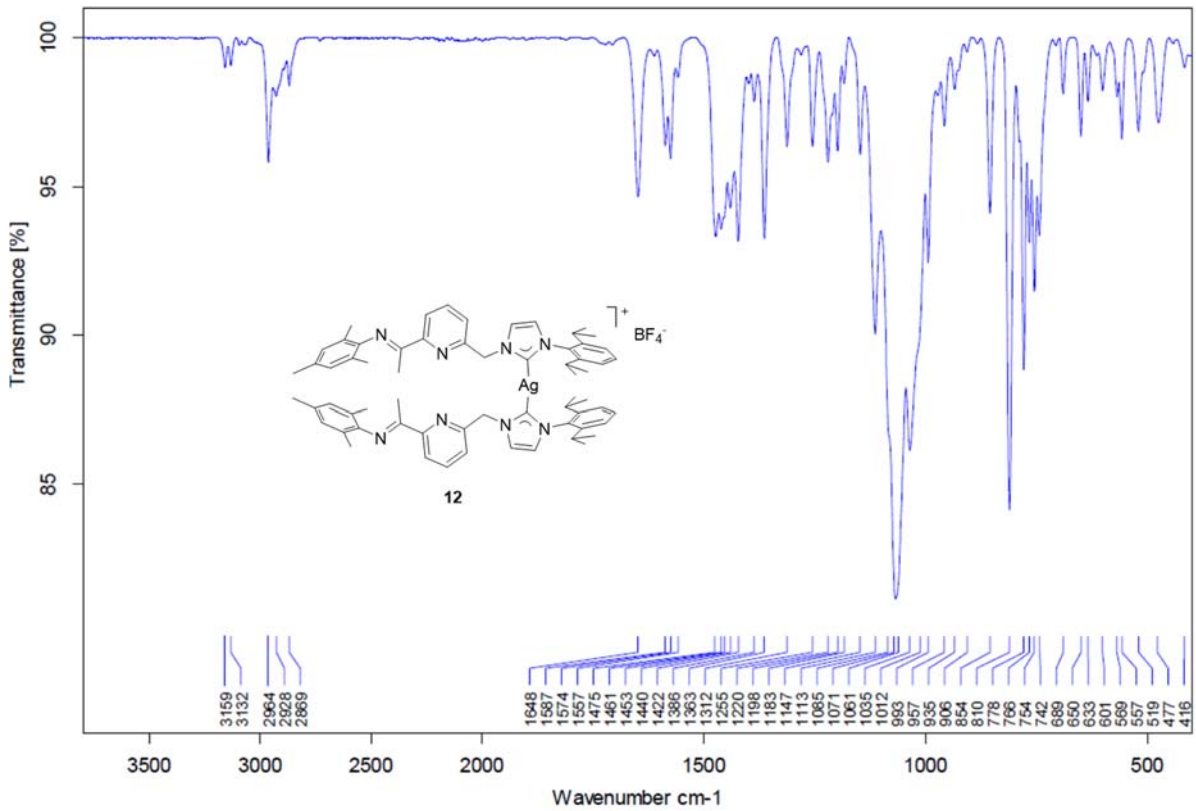

Figure S51. IR spectrum of complex **12**.

IV.6. Complex 13

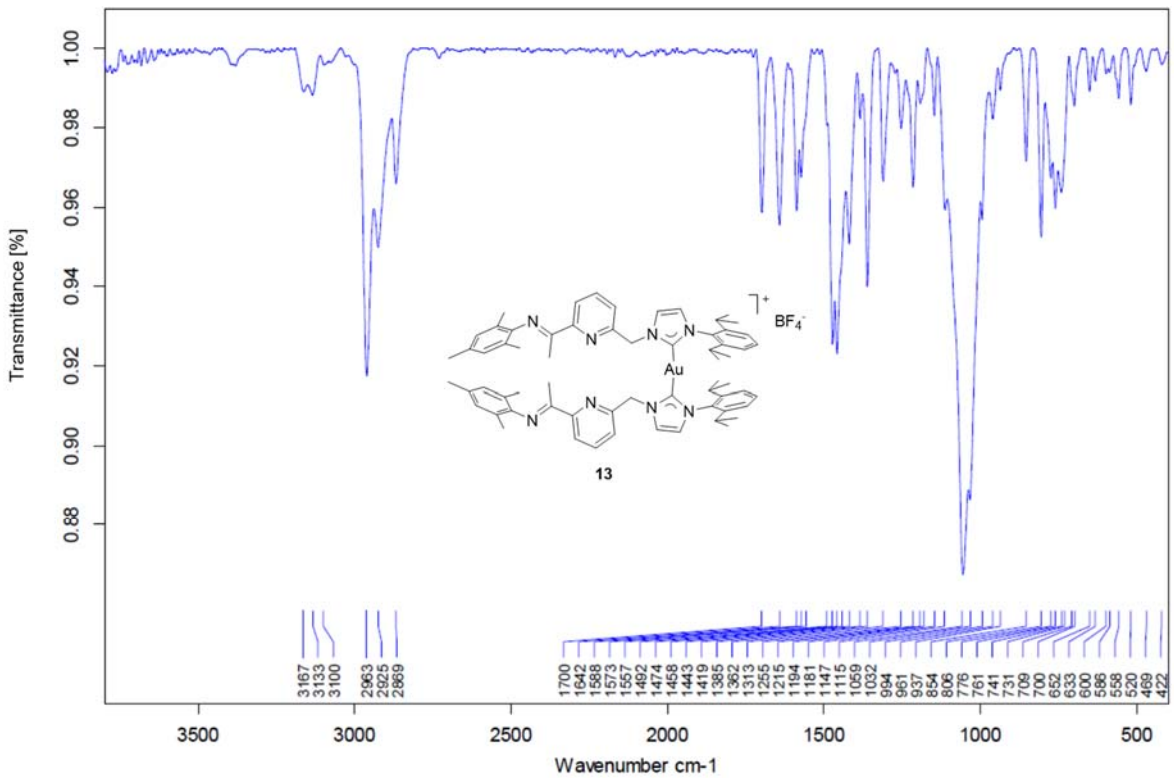

Figure S52. IR spectrum of complex **13**.

IV.7. Complex 14

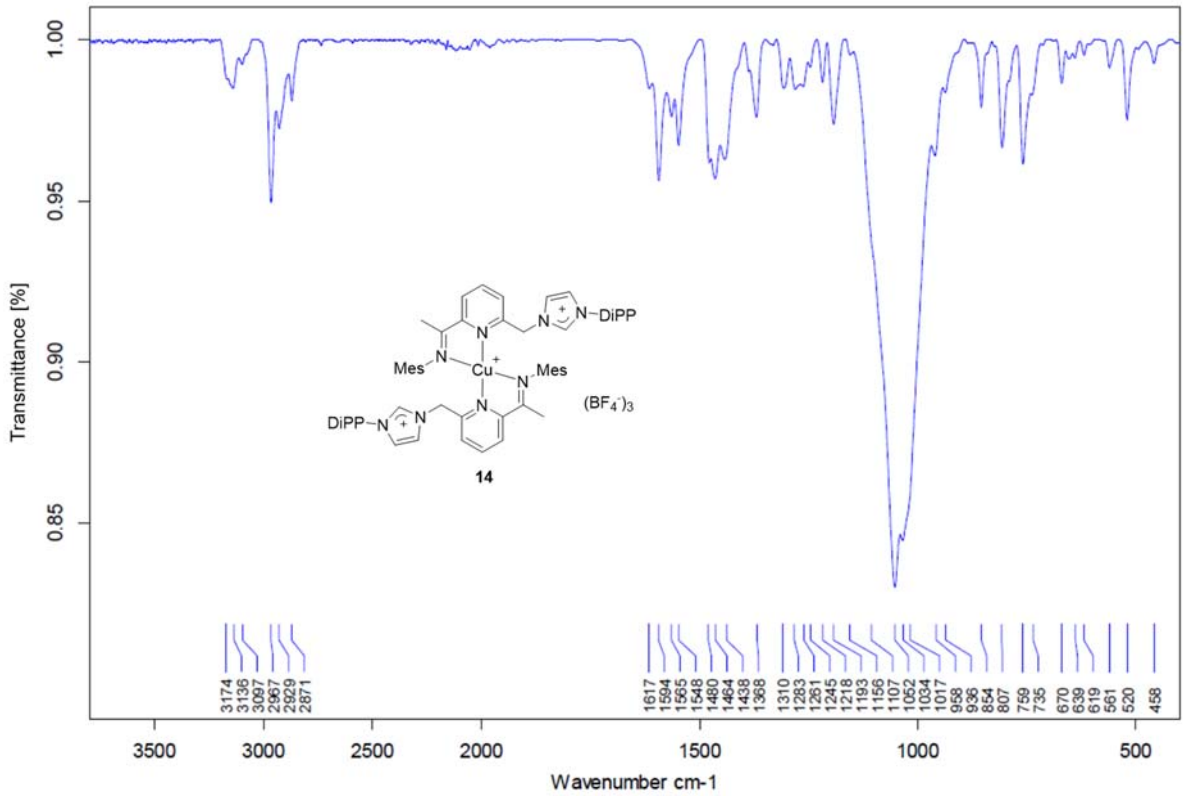

Figure S53. IR spectrum of complex **14**.

IV.8. Complex 15

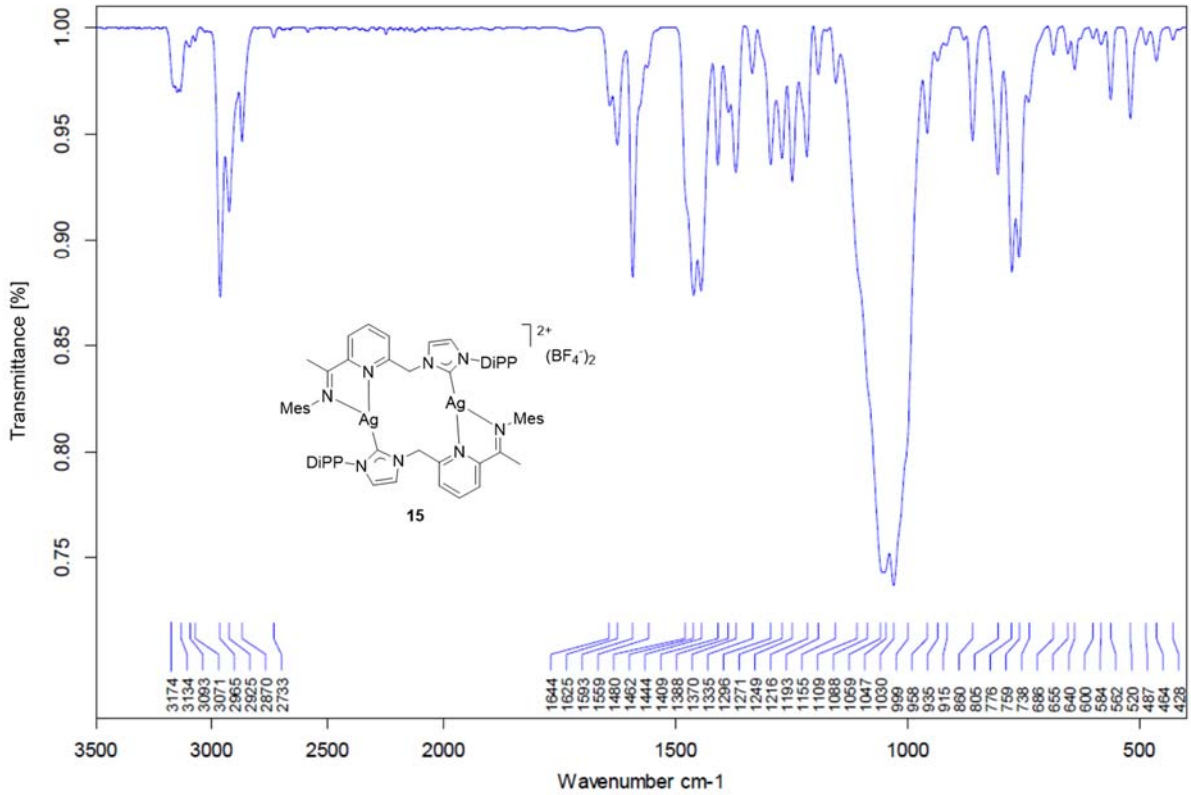

Figure S54. IR spectrum of complex **15**.

IV.9. Complex 16

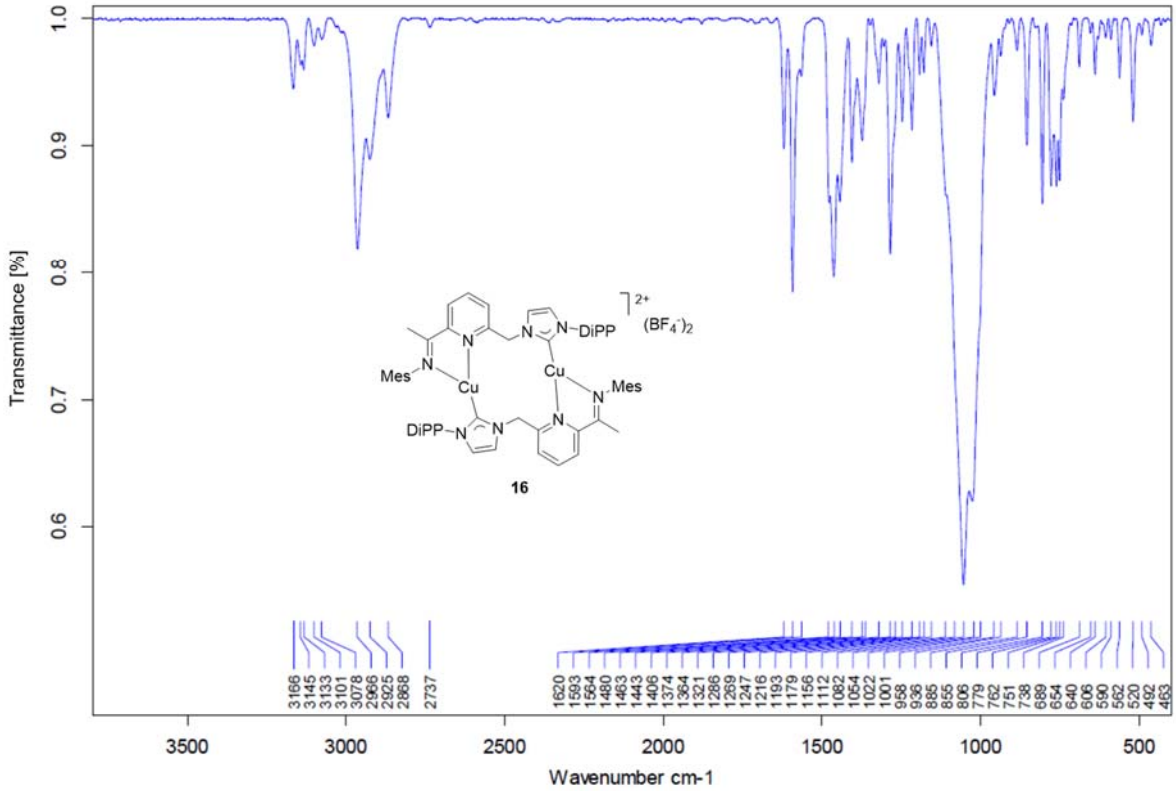

Figure S55. IR spectrum of complex **16**.

IV.10. Complex 17

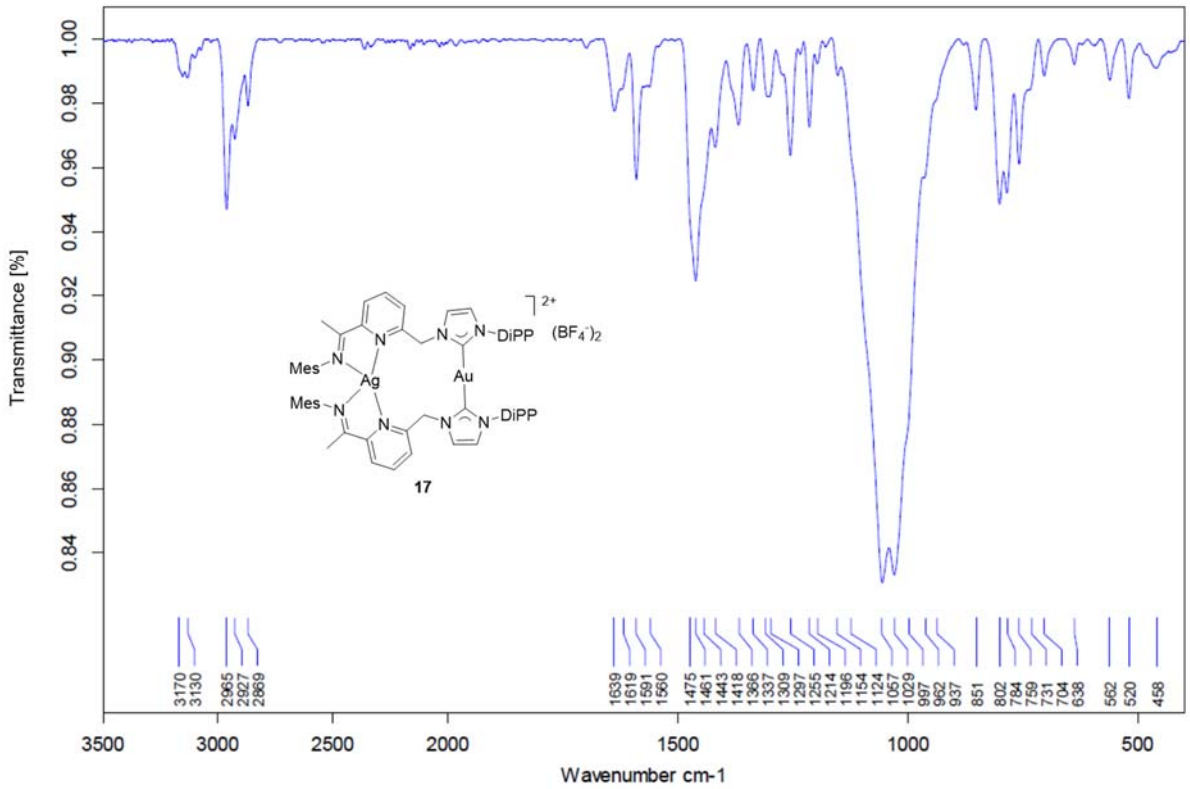

Figure S56. IR spectrum of complex **17**.

IV.11. Complex 18

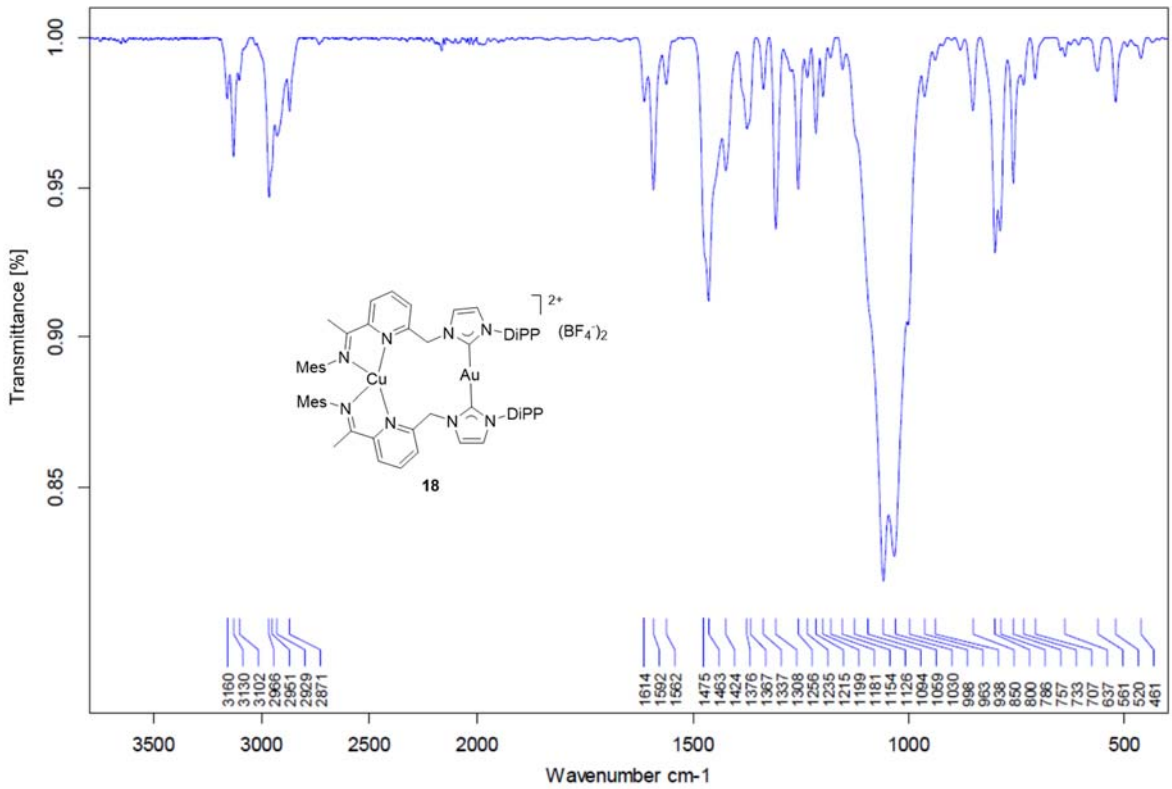

Figure S57. IR spectrum of complex **18**.

V. UV-VIS SPECTRA

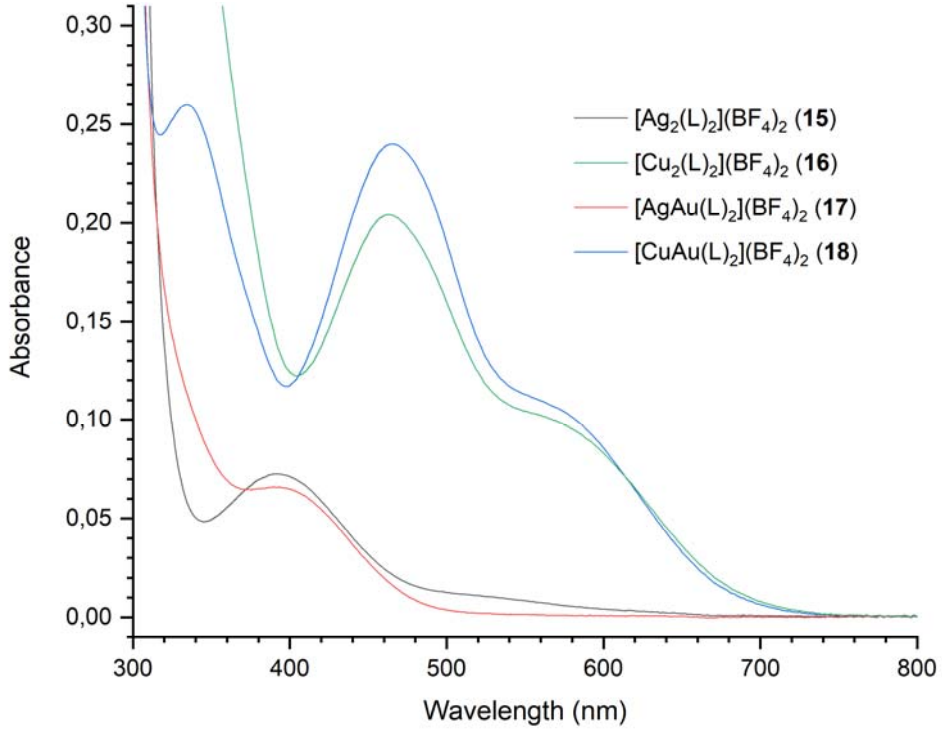

Figure S58. UV-vis absorption spectra of the dinuclear complexes **15**-**18** in the range 300-800 nm, recorded at a concentration of 0.10 mg mL^{-1} in CH_2Cl_2.

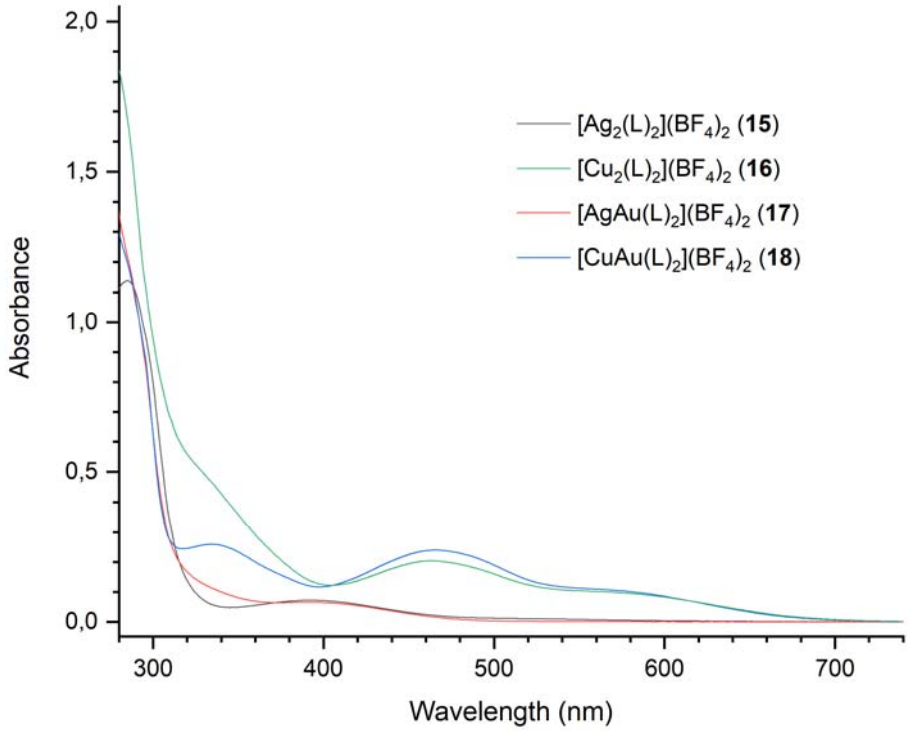

Figure S59. UV-vis absorption spectra of the dinuclear complexes **15**-**18** in the range 280-740 nm, recorded at a concentration of 0.10 mg mL^{-1} in CH_2Cl_2.

VI. PHOTOLUMINESCENCE

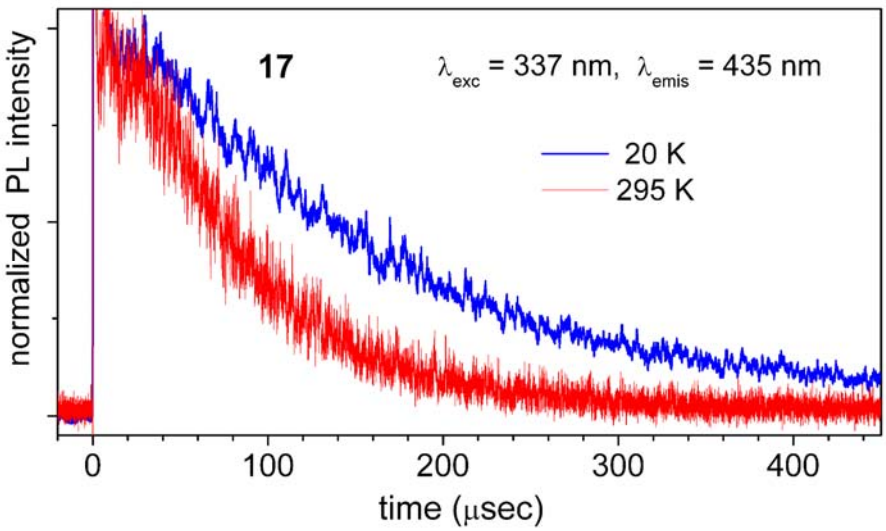

Figure S60. PL decay of solid (polycrystalline) complex **17** excited with a nsec-pulsed nitrogen laser at 337 nm and recorded at 435 nm at low and ambient temperatures. The decay traces can be fitted with monoexponential curves with τ = 154 and 69 µsec at 20 and 295 K, respectively.

VII. REFERENCES

(1) (a) Parks, J. E.; Wagner, B. E.; Holm, R. H. Syntheses Employing Pyridyllithium Reagents: New Routes to 2,6-Disubstituted Pyridines and 6,6'-Disubstituted 2,2'-Bipyridyls. *J. Organomet. Chem.* **1973**, *56*, 53-66. (b) Bolm, C.; Ewald, M.; Felder, M.; Schlingloff, G. Enantioselective Synthesis of Optically Active Pyridine Derivatives and C_2-Symmetric 2,2'-Bipyridines. *Chem. Ber.* **1992**, *125*, 1169-1190.

(2) Bianchini, C.; Giambastiani, G.; Rios, I. G.; Meli, A.; Oberhauser, W.; Sorace, L.; Toti, A. Synthesis of a New Polydentate Ligand Obtained by Coupling 2,6-Bis(imino)pyridine and (Imino)pyridine Moieties and Its Use in Ethylene Oligomerization in Conjunction with Iron(II) and Cobalt(II) Bis-halides. *Organometallics* **2007**, *26*, 5066-5078.

(3) Bur, D.; Corminboeuf, O.; Cren, S.; Fretz, H.; Grisostomi, C.; Leroy, X.; Pothier, J.; Richard-Bildstein, S. Preparation of Aminopyrazole Derivatives as ALXR Receptor Agonists. WO2009077954, 2009.